Journal of Materials Research and Technology 39 (2025) 3270–3291

Contents lists available at ScienceDirect

Journal of Materials Research and Technology

journal homepage: www.elsevier.com/locate/jmrt

(Semi-)Solid-state joining of aluminium and titanium alloys – A critical review

Felix Grassel [a,*], Lasse Malaske [b], Marius Hoffmann [a], Benjamin Klusemann [a,b]

[a] Institute of Materials and Process Design, Helmholtz-Zentrum Hereon, Max-Planck-Strasse 1, Geesthacht, 21502, Germany
[b] Institute for Production Technology and Systems, Leuphana University Lüneburg, Universitätsallee 1, Lüneburg, 21335, Germany

ARTICLE INFO

Keywords:
Aluminium
Titanium
Diffusion
Intermetallic compounds
Solid-state welding

ABSTRACT

Joining dissimilar lightweight alloys is one key challenge for achieving cost and weight reduction in structural parts especially for transport applications. In this work, the state of the art in joining of aluminium and titanium alloys via solid-state techniques is critically analysed and discussed, particularly regarding generalisable statements in terms of process- and material-related findings. Processes are compared regarding their time-temperature-cycles and mechanical impact on the materials. Focus is laid on the interface evolution, diffusion, formation of intermetallic compounds as well as the influence of alloying elements. Findings are critically reviewed, discrepancies and knowledge gaps regarding diffusion coefficients, preconditions for and influence of intermetallics, and the influence of plastic deformation highlighted. Although there is no systematic experimental investigation of fundamental factors available in the literature, it can be stated that mechanical deformation has a strong accelerative effect on the interdiffusion and lowers the diffusion start temperature significantly. Alloying elements like Al, Cu and Si decrease while Mg accelerates the interdiffusion of Al and Ti. $TiAl_3$ is typically the primary intermetallic compound to form in solid-state processes but is found to be no precondition for firm bonding.

Abbreviations

cp	commercially pure
DB	Diffusion Bonding
EDS	Energy-Dispersive X-Ray Spectroscopy
EW	Explosive Welding
FMB	Friction Melt Bonding
FSBW	Friction Stir Butt Welding
FSJ	Friction Stir Joining
FSLJ	Friction Stir Lap Joining
FSLW	Friction Stir Lap Welding
FSW	Friction Stir Welding
FW	Friction Welding
IMC	Intermetallic Compound
LSS	Lap-Shear Strength
PWHT	Post-Weld Heat-Treatment
RB	Roll Bonding
refill FSSW	refill Friction Stir Spot Welding
SSSJ	(Semi-)Solid-State Joining
TEM	Transmission Electron Microscope
TLPB	Transient Liquid Phase Bonding
UTS	Ultimate Tensile Strength
UW	Ultrasonic Welding
WB	Weld-Brazing
XRD	X-Ray Diffraction

1. Introduction

Aluminium and titanium alloys are two of the most promising materials for lightweight construction especially in the transportation industry. As sustainability, fuel-saving and resource-efficiency regarding materials and production capacities gain importance, differential lightweight construction is one key feature to address these challenges. Both material systems have specific advantages such as low cost and low density for aluminium and high strength and high temperature stability for Ti alloys. Additionally, they are able to compensate for specific disadvantages of each other, such as low creep resistance for Al alloys

* Corresponding author.
E-mail addresses: felix.grassel@hereon.de (F. Grassel), lasse.malaske@leuphana.de (L. Malaske), marius.hoffmann@hereon.de (M. Hoffmann), benjamin.klusemann@leuphana.de (B. Klusemann).

https://doi.org/10.1016/j.jmrt.2025.09.239
Received 24 June 2025; Received in revised form 19 September 2025; Accepted 25 September 2025
Available online 26 September 2025

and high costs for Ti.

Possible applications are currently considered, especially in aeronautics, where weight reduction has the highest impact on operational costs. One case is the implementation of a hybrid seat rail, where the upper part (Ti) is in contact with moisture, salt and other corrosives on the cabin floor, while the lower part (Al) can be protected by coatings [1]. Furthermore, in highly stressed regions, Al skin plates are reinforced with Ti profile stringers, which are currently riveted but might also be joined by welding [2]. In wing structures, weight reduction can be achieved by dissimilar structures of Ti plates filled with Al honeycombs [3]. Corrosion and wear resistance as well as high strength are reasons for the local application of Ti parts, so that further applications are conceivable in which suitable welding processes can replace current concepts.

As shown, hybrid structures of these materials are required but also technologically challenging; first, because of the differing thermo-mechanical properties (solidus temperature, thermal conductivity, coefficient of thermal expansion) and second, also due to their chemical affinity [4,5], resulting in brittle intermetallic compounds (IMC). In this regard, fusion welding techniques, such as arc welding [6], laser welding [7–10] or electron beam welding [11,12], have been investigated but resulted in defects such as uneven, intricate weld pool profiles, high residual stresses, cracks, and microporosity [13]. Latest attempts overcome these issues partially by using high-alloyed filler metals but achieve only 50 % of the base material strength [14]. Al–Ti intermetallic compounds have high strength, however, their brittleness deteriorates the ductility, tensile strength and fatigue strength of welded structures [15]. Several approaches have been applied in the last decades to overcome these issues. Especially, solid-state joining technologies are promising in reducing excessive heat input during joining, because mechanical stirring increases diffusivity at low temperatures [16]. Relevant solid-state techniques for joining Al–Ti can be classified according to Gadakh et al. [13] as Pressure Welding, Friction Stir Butt Welding, Friction Stir Lap Welding, Friction Stir Spot Welding, Friction Welding, Diffusion Bonding, Explosive Welding, Accumulative Roll Bonding, Brazing, Electromagnetic Welding, Friction Melt Bonding, Transient Liquid Phase Bonding, Diffusion Brazing as well as hybrid processes, namely ultrasonic assisted friction- and pressure based welding, heating and cooling assisted processes and combinations of the above-mentioned processes. Additionally, semi-solid-state joining or weld-brazing techniques like electron-beam [17] or laser weld-brazing [1] and arc weld-brazing [18], where only the Al alloy was locally molten, have been investigated.

Although there are over 200 publications on the topic of solid-state joining of Al and Ti, their focus is mostly limited on evaluating individual effects and optimising process parameters for one single pair of materials and one joining configuration (e.g. geometrical and environmental conditions). Based on this, some researchers have compared process-specific findings, especially regarding process parameters. For example, Cooke et al. [19] reviewed diffusion bonding of Al and Ti, while Jain et al. [20] and Khalafe et al. [21] focused on Friction Stir Welding (FSW). However, general applicable statements based on fundamental physical and chemical principles are almost not found [22].

Hence, other dissimilar material combinations need to be taken into account and analysed for parallels. As the differences in properties like solidus temperature and yield strength between Al and steel are comparable to those of Al and Ti, although a bit lower for steel in comparison to Ti, the combination of Al and steel is of special interest. Beygi et al. [23] published a comprehensive review on dissimilar FSW of Al and steel, while He et al. [24] compared interface evolution in joining of Al and Ti with Al and steel for Ti–Al-steel (TC4-LF6-1Cr18Ni9Ti) diffusion couples. For this reason, some similarities in interface evolution can be estimated albeit the intermetallic formation of Fe and Al is much faster. Chemical reactions and the formation of intermetallic phases (especially $TiAl_3$) during solid-state [25] and semi-solid-state reactions [26] are proven to occur. Despite that, because of the limited reaction time and low temperature in solid-state joining processes, also diffusion-based bonding or micro-mechanical interlocking are assumed to play an important role.

Within this manuscript, observations regarding the interface evolution are compared over a wide range of processes, alloys and parameters to generate a knowledge-based understanding of fundamental mechanisms during (semi-)solid-state joining (SSSJ) of Al and Ti alloys as well as to reveal current knowledge gaps. First, the principles of relevant solid-state processes are explained and categorised regarding their characteristics. Then, the microstructural evolution is described from the optical appearance over the mechanisms of diffusion to the formation of intermetallic compounds. Based on this, the observations regarding mechanical properties are summarised. At last, energy input and alloying elements as the two main influencing parameters are reviewed to give a broad overview of principles in SSSJ of Al and Ti. Based on the critical review of these aspects, future research directions are identified.

2. Processes

Several processes have been investigated in the past decades for SSSJ of Al and Ti. The most frequently reported processes are listed and classified hereinafter.

2.1. Diffusion bonding

Diffusion bonding (DB) or welding – patented already in 1964 [27]– uses the principle of solid-state diffusion to achieve bonding strength equal to the base material. The process is characterised by a relatively long duration (~1 h) but enables homogeneous properties and the absence of residual stresses in the joined workpiece. The main process parameters are pressure, temperature and time of contact. Evenness and cleanness of the faying surfaces are an essential precondition for sound bonding as all intermediate spaces or impurities would act as diffusion barriers [28]. During welding, the workpieces are heated up to 0.5–0.7 of the solidus temperature under static loading, see Fig. 1 a). The process is carried out under vacuum condition to avoid oxidation [29].

2.2. Transient Liquid Phase Bonding

Transient liquid phase bonding (TLPB) uses the same principles as DB, but the temperature is sufficient to melt a thin film at the interface of the joining partners, see Fig. 1 b). This is achieved by introducing a thin foil of an eutectic phase or a material that forms an eutectic with the base metal [30].

2.3. Roll bonding

Roll bonding (RB) achieves joint formation by parallel application of pressure on the interface and plastic deformation of the bonding partners, see Fig. 1 c). It can be conducted at room temperature (cold roll bonding), where the effect of strain-induced diffusion is maximised, but higher force is needed, or at diffusion temperatures (hot roll bonding), where the material behaves softer but also deterioration of the microstructure (grain coarsening and dissolution of phases) can occur. Main process parameters are the degree of deformation measured by the thickness reduction, the number of rolling steps and (in case of hot roll bonding) the process temperature. Fabrication of multi-layered structures is referred as accumulative roll bonding [31].

2.4. Explosive Welding

Explosive welding (EW) or cladding – invented in 1957 [32] – uses an explosion to create a high-velocity jet of the surface layer of one partner to remove the surface layer of another and to achieve intimate

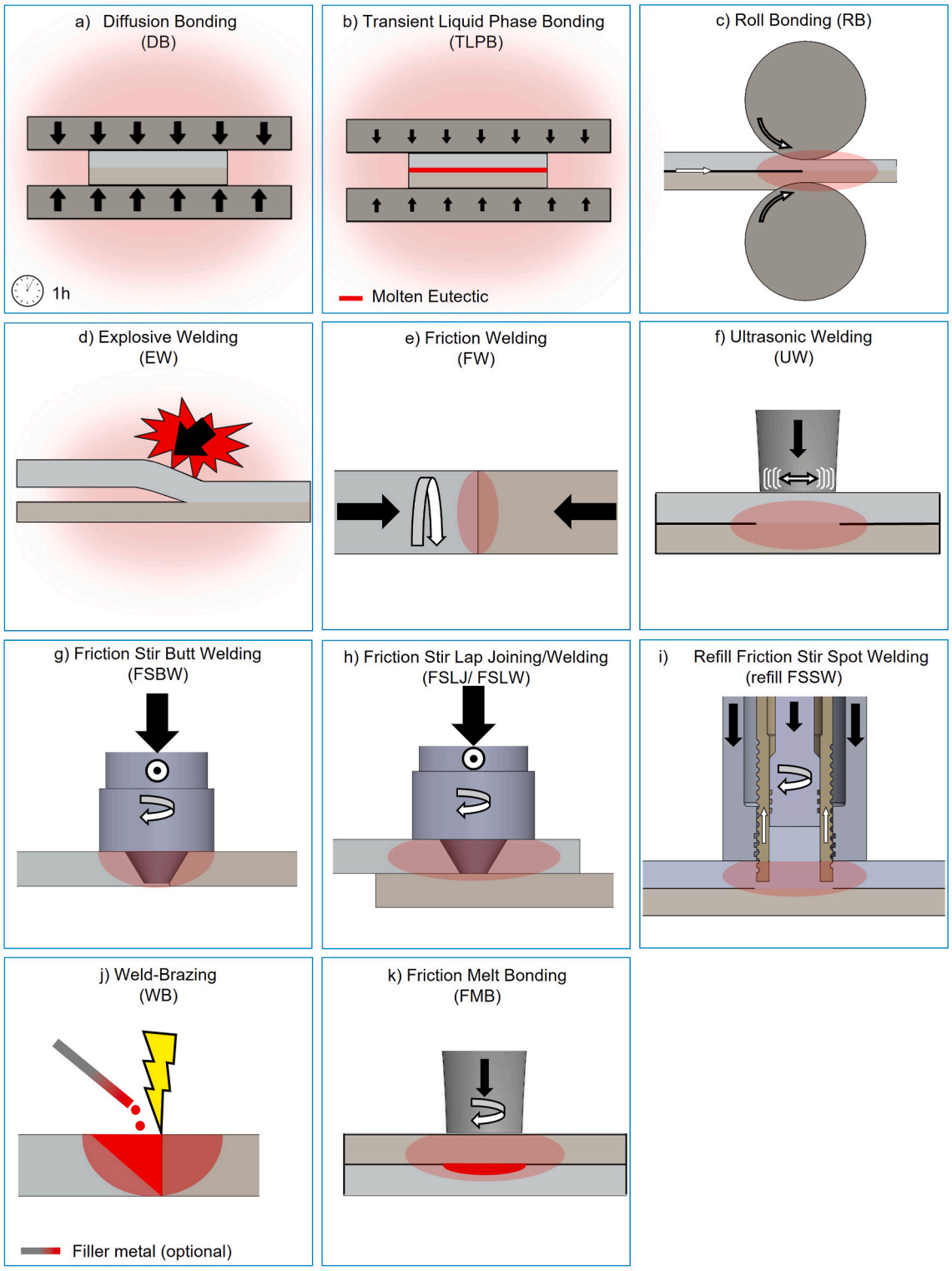

Fig. 1. Schematic illustration of the reviewed (semi)-solid-state joining processes for joining Al and Ti.

contact, see Fig. 1 d). The main process parameters are the amount of explosive and the initial gap size between the joining partners. It is characterised by an extremely short process time with high impact pressure at the line of contact between the joining partners. This causes the material to behave more like an inviscid fluid than a solid [32].

2.5. Friction Welding

Friction welding (FW) – patented in 1956 [33] – is based on the frictional heat generated between two components during their relative movement while being pressed against each other. By abrupt stopping of the motion at a defined degree of deformation, the activated surfaces are forced on each other to form a joint, see Fig. 1 e). Consequently, the main process parameters are the relative speed in the friction phase as

well as force and duration in both the friction and forging phases. The process times are relatively short (~10 s) [33].

2.6. Ultrasonic welding

Ultrasonic welding (UW) – first reported in 1953 [34] – is based on the same principles as FW, but the relative movement is applied oscillatory with a high frequency either linear or circular, see Fig. 1 f). This makes the process applicable to almost all workpiece geometries [34].

2.7. Friction stir butt joining/welding and friction stir lap joining/welding

Friction stir welding (FSW) – patented in 1991 [35] – uses a non-consumable rotating tool plunged into the workpiece to plasticise and stir the welding partners. As the tool travels along the weld line, a linear weld is formed. The main process parameters are rotational and translational speed of the tool as well as the axial force or position of the tool. The process can be applied in butt- (FSBW, see Fig. 1 g)) and lap- (FSLW, see Fig. 1 h)) configuration [36]. If the tool only stirs in one partner, the process is referred to below as Friction Stir Joining (FSJ).

2.8. Refill friction stir spot welding

Refill friction stir spot welding (refill FSSW) – patented in 2001 [37] – is a relatively new solid-state joining/welding process based on the FSW concept, whereby a non-consumable tool consisting of two movable parts and one stationary part is used. While the stationary clamping ring clamps down the welding partner, the movable probe (previously named pin) and shoulder (previously named sleeve) rotate and move vertically inside the clamping ring. Here the shoulder plunges downwards into the workpiece, plasticizes the material and displaces it into the cavity left by the pin moving in reverse direction. Subsequently, both parts retract to the original surface level whereby no exit hole is generated, see Fig. 1 i). The process can be described via the clamping force, the rotational speed of probe and shoulder, the plunge and retracting speed and depth as well as the dwell time between plunging and retracting of the tool. Refill FSSW is mainly used in overlap configuration for similar and dissimilar materials [38].

2.9. Weld-brazing

Weld-brazing (WB) is a fusion-based joining technique for materials with highly unequal fusion temperatures. It's based on the principles of brazing while one material acts as the brazing solder, see Fig. 1 j). Main process parameters are the energy per unit length and the welding speed. An additional filler material can be used to mitigate the loss in mechanical properties due to the melting and solidification of the molten joining partner. Energy input is often provided by laser or electron beam but also by electrical arc or current.

2.10. Friction Melt Bonding

Friction melt bonding (FMB) – patented in 2013 [39] – combines Friction Stir Spot Welding and TLPB. Friction is applied to the material with the higher solidus temperature by a non-consumable flat cylindrical tool and the generated heat partially melts the surface of the other material to form a joint by solid-liquid diffusion, see Fig. 1 k). The main process parameters are the axial force as well as the rotational and translational speed of the tool [40].

2.11. Classification of processes

Two ways of heat input can be distinguished in these kind of processes: Temperature-driven processes, where heat is provided by resistance heating (DB, WB, TLPB) or combustion (EW), and deformation-driven processes, where heat is produced from friction between or in the workpieces (FW, RB) or between a tool and the materials (FSW, refill FSSW, FMB), see Table 1.

The processes can also be classified regarding the average joining time, which ranges from milliseconds for EW to minutes and hours for TLPB and DB, see Fig. 2. It is interesting to note that all deformation-driven processes have comparable joining times in the range of seconds, while the temperature-driven processes have either extremely low or comparatively high joining times. Low joining times are caused by the mechanical impact (EW) and/or the high peak temperatures of the molten Al (EW, WB), whereas high joining times (TLPB and DB) are caused by the lack of an accelerative effect of material flow.

Despite the fact that most of these processes are in general classified as "solid-state", as there is no significant melt pool in the joining zone, some of these processes involve partial melting of the aluminium alloy and should therefore be named as "semi solid-state". Partial melting is inevitable in TLPB, WB and FMB, but there is also evidence for partial melting in FSBW and FSLW.

Regarding the deformation-driven processes, plastic deformation is mainly limited to the Al side due to the significantly higher strength of Ti. Severe plastic deformation of both Al and Ti is only found in RB, FSLW and FSBW. While in RB the incompressibility of Al leads to a nearly similar deformation of Al and Ti [41], for FSLW and FSBW weakening of the joint due to unbonded Ti flakes, cracking and voids due to insufficient material flow are reported.

3. Microstructure

Besides mechanical properties, microstructural evolution is the second main point of interest in recent research on joining of Al and Ti. Focus in deformation-based process is laid on interface topography, changes in base metal structure due to thermo-mechanical influence – for example Dressler et al. [42] observed recrystallisation in Ti6Al4V during FSBW to AA2024 –, and structural defects. For all joining processes, the thickness of diffusion and intermetallic layers are of special interest, therefore they are analysed separately in the sections hereafter.

Kim and Fuji [15] stated that for an intermetallic compound layer in FW and post-weld heat-treatment (PWHT), a thickness of 5 μm is critical to deteriorate the mechanical properties. However, the results in SSSJ show that interface thicknesses in this range are rarely reached. For example, Choi et al. [43] found intermetallic layers in a range of 20–60 nm after FSBW of cp Al and Ti, see Fig. 3. In contrast, Foadian et al. [44] found non-uniformly distributed IMCs with a thickness of 9.5 μm after EW for the same material combination, see Fig. 4. Additionally, in FSW, the interface might consist of laminate structures of multiple phases formed by the oscillating material flow [45]. Geyer et al. [46] found these lamellas to be $TiAl_3$/TiAl and Ti_3Al/TiAl in FSLW of AA2024 to Ti6Al4V, see Fig. 5. The microstructure is influenced especially by the time-temperature cycle, the degree of plastic deformation and the applied pressure. Varying the welding conditions in FSLW of AA6061

Table 1
Classification of (semi-)solid-state joining techniques by energy input.

	Solid-State	Semi-Solid-State
TEMPERATURE-DRIVEN	Diffusion Bonding (DB)	Explosive Welding (EW) Weld-Brazing (WB) Transient Liquid Phase Bonding (TLPB)
DEFORMATION-DRIVEN	*Friction Stir Butt Joining (FSBJ)*[a] Friction Stir Lap Joining (FSLJ) Refill Friction Stir Spot Welding (refill FSSW) Friction Welding (FW) Roll Bonding (RB) Ultrasonic Welding (UW)	Friction Stir Butt Welding (FSBW) Friction Stir Lap Welding (FSLW) Friction Melt Bonding (FMB)

[a] (no literature on Al–Ti joints available yet).

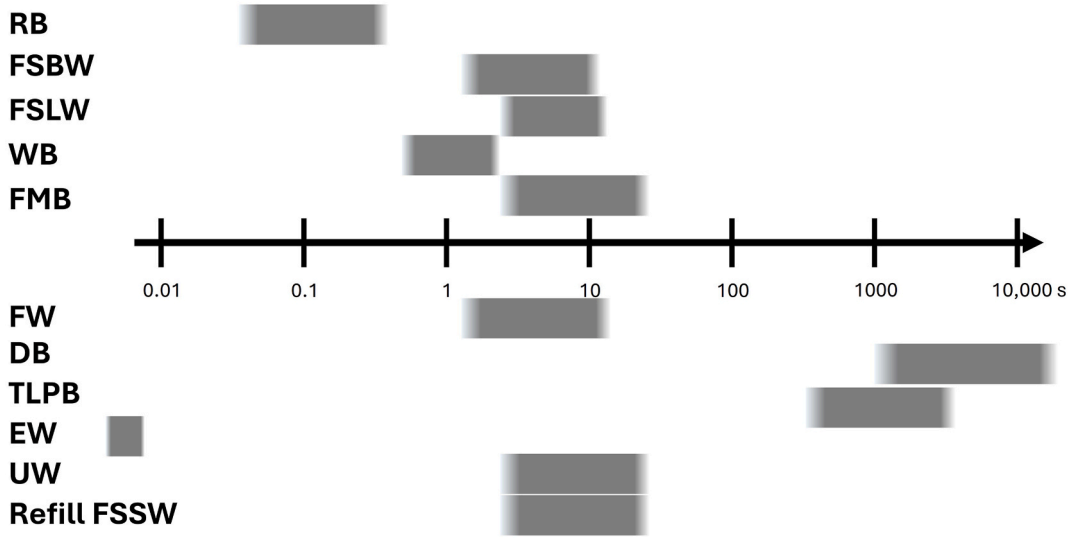

Fig. 2. Schematic of average joining times of SSSJ-processes.

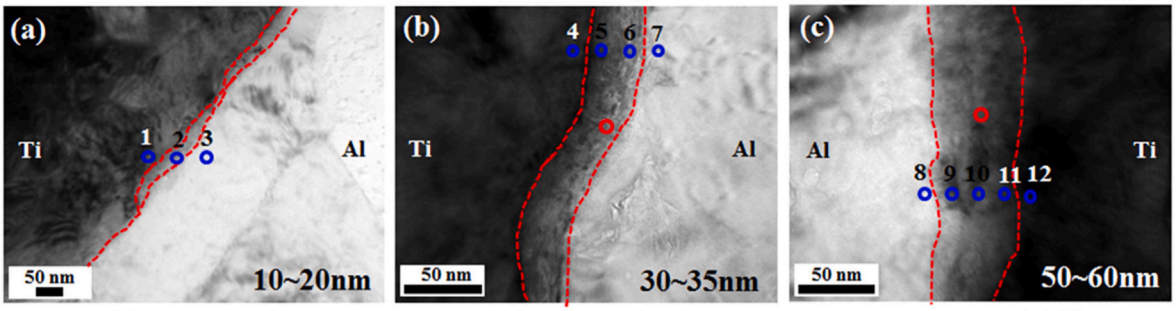

700 rpm	(at.%)	
	Ti	Al
1	91.57	8.43
2	27.91	72.09
3	3.70	96.30

800 rpm	(at.%)	
	Ti	Al
4	90.05	9.95
5	48.57	51.43
6	22.37	77.63
7	1.05	98.95

900 rpm	(at.%)	
	Ti	Al
8	1.26	98.74
9	28.93	71.07
10	50.18	49.82
11	78.49	21.51
12	92.43	7.57

Fig. 3. TEM images of intermetallic layers after FSBW of cp Al and Ti at rotation speeds of a) 700, b) 800 and c) 900 rpm ranging from 20 to 60 nm, which is indicated by the number on the right in the images. Chemical composition indicates the formation of TiAl3, TiAl and Ti3Al. Reprinted from Ref. [43] with permission from Elsevier.

and Ti6Al4V, Yu et al. [22] observed two types of interfaces, named 'diffusive interface' for low heat input and 'mixed interface' for high heat input, see Fig. 6. They measured interface temperatures on the advancing side close to the stir zone and found them to be in the range between 471 and 564 °C. While the diffusive interface is characterised by a flat topography and a homogeneous $TiAl_3$ layer, the mixed interface has a rough topography and TiAl is formed from $TiAl_3$ due to excessive heat input [22].

Regarding the interface topography, plastic deformation of the Ti is not only caused by the stirring action of a tool but also by the Al material flow [47]. Kar et al. [16] found additional slip systems to contribute to the plastic deformation in Ti above 400 °C. Additionally, Ji et al. [48] investigated the flow stress of Ti6Al4V as function of temperature and found it to be reduced to ~ 50 % in the SSSJ-temperature range (600–700 °C) compared to room temperature. While Ti6Al4V is relatively brittle at room temperature, it exhibits superplasticity at temperatures above 650 °C [49], which is in the range of SSSJ, i.e. plastic deformation of the Ti is likely to occur [22].

Some observations additionally suggest that the crystallographic orientation of the base metal grains also influences the intermetallic reaction. Kalinenko et al. [50] concluded that IMC nucleation was influenced by diffusion anisotropy due to the particular crystallographic orientation of the Ti. On the other hand, Ramana et al. [51] investigated the Al structure and found diffusion of Ti sputtered on Al single crystals to start at 400 °C for Al crystals with the (110) plane oriented parallel to the interface but above 450 °C also on crystals with a (100) and (111) orientation. Latter crystals have up to 42 % higher packing density in diffusion direction. Here, more energy is needed to allow the diffusion of Ti atoms into the Al lattice as the higher packing density acts as a larger kinetic barrier. This might explain the non-uniformity of the IMC in as-welded condition as recognised by some researchers [44]. It should be noted that the diffusion start temperatures are significantly lower

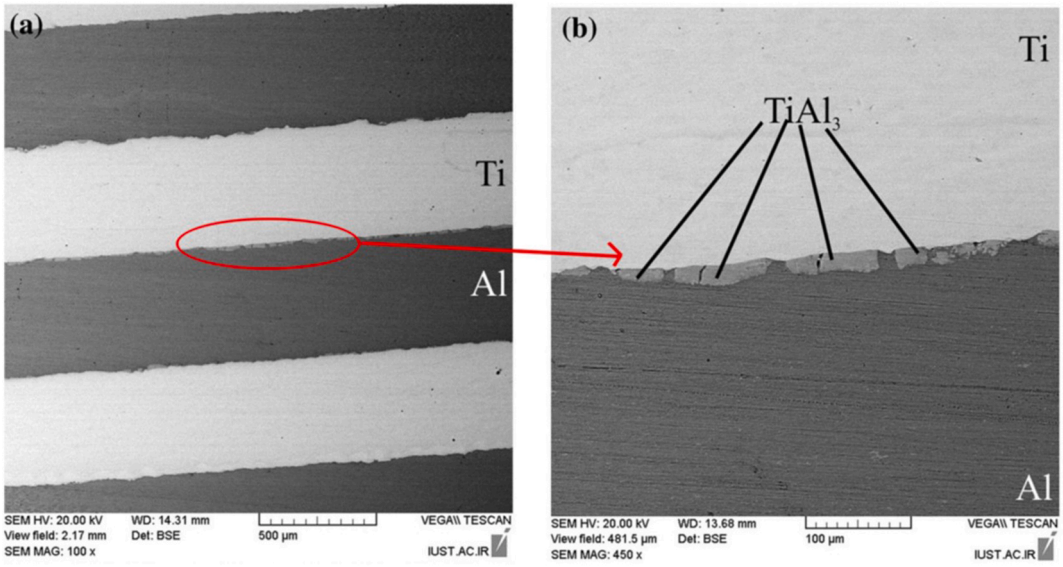

Fig. 4. SEM macrograph of non-uniformly distributed IMCs with a thickness of 9.5 µm after EW of cp Al and Ti. Reprinted from Ref. [44] with permission from Springer Nature.

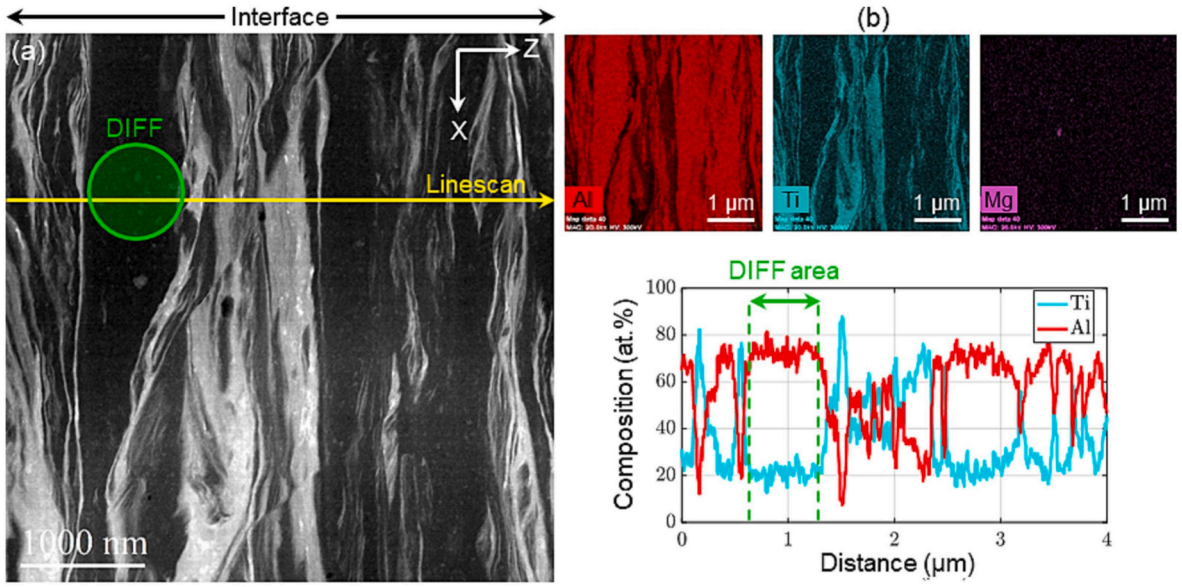

Fig. 5. TEM images (a) and EDS-mapping (b) of TiAl3/TiAl and Ti3Al/TiAl lamellas in FSLW of AA2024 to Ti6Al4V formed due to the mechanical stirring of both joining partners. Reprinted from Ref. [46] with permission from Elsevier.

than in experiments using cp alloys because of the lack of inhibiting alloying elements as well as the high amount of grain boundaries that lead to a nearly amorphous character of the sputtered layer [52].

From the above-mentioned investigations, it can be concluded that in the interface IMC-layers in a range from non-detectible to around 10 µm as well as multi-phase laminates (especially after FSW) are found. Plastic deformation and partial recrystallisation of Ti is possible at the upper limit of temperature range in SSSJ of Al and Ti (600–650 °C), so the interface topography might change from flat (diffusive) to mixed with increased energy input, see Fig. 6. Non-uniformity of diffusion is explained by inhomogeneity of the Al and Ti crystal structure, further aspects are reviewed in the following sections.

4. Diffusion

Inter-diffusion in pairs of different metals is caused by the concentration gradient of elements in the diffusion partners. For pure metals, diffusion can be described by Fick's second law [53]. As a perfect crystal structure provides no possibility for atomic movement, lattice defects (especially vacancies) are a fundamental requirement for the diffusion of atoms in metals. While atoms move within a homogeneous crystal structure (monocrystalline) through the movement of dislocations, called lattice diffusion, in inhomogeneous structures (polycrystalline), they might (if the atomic radius is comparable) move likewise within the crystal structure but also along grain boundaries, called grain boundary diffusion [54]. Time, temperature, pressure and degree of deformation are the main parameters determining the rate of diffusion. In DB of similar metals, process temperatures of 0.5–0.8 of the solidus temperature (i.e. 700-1300 °C for Ti and 200–500 °C for Al) are applied [53]. Wei et al. [55] determined the growth of the diffusion layer in the Al–Ti system to be proportional to the square root of diffusion time as shown in Fig. 7 and with a time delay before the start of

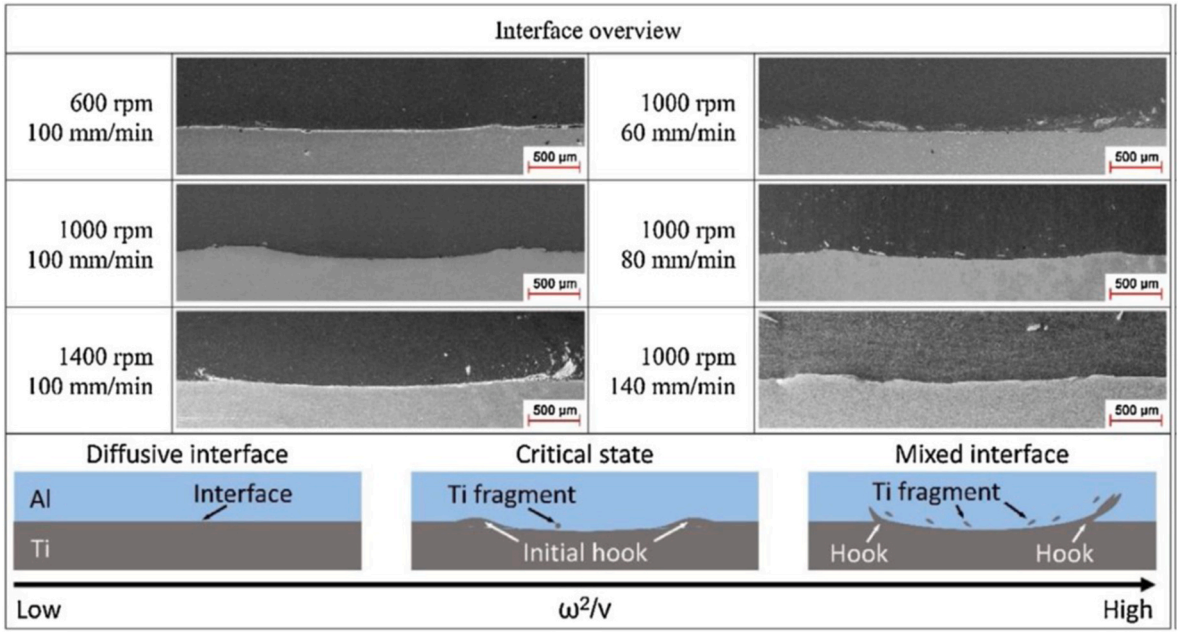

Fig. 6. Interface evolution in FSLW of AA6061 and Ti6Al4V depending on welding parameters, showing the transition from diffusive to mixed interface characterised by increasing plastic deformation of the Ti surface and formation of Ti particles with increasing rotational speed (left) and decreasing welding speed (right), reprinted from Ref. [22] with permission from Elsevier.

diffusion, which decreases with increasing temperature between 600 and 650 °C.

Interdiffusion between Al and Ti is a necessary requirement to achieve the stoichiometry for the formation of intermetallic compounds. However, especially at low temperatures (below 550 °C), some investigations assume bonding without formation of intermetallic phases [42,56,57], as there was no evidence for IMC formation even on a 2 nm scale [57].

In DB of Al and Ti, a minimum energy input, defined by peak temperature and holding time, is required. However, the influence of the welding temperature is found to be significantly higher than of the welding time [55]. Wilden et al. [58] found the minimum joining temperature for Ti Gr.2 and cp-Al to be 520 °C for process times below 60 min, while 550 °C is needed for times below 10 min. This is in accordance with findings by Rajakumar and Balasubramanian [59] for AA7075 and commercially pure titanium, where the optimum process parameters regarding tensile strength were 37 min @ 510 °C. As these temperatures are equal to only 40 % of the Ti solidus temperature, the diffusion activity of Ti is expected to be low. Furthermore, pressure during DB is required to generate intimate contact between the joining partners and to break up the oxide layers, which are always present in industrial and lab environments [25].

While some researchers expect Al to be the only diffusion element [4], others found both Al and Ti to be diffusing at various temperatures [60], especially, if plastic deformation of Al is involved [61]. Liu et al. [61] listed several investigations that showed diffusion mainly in either Ti [54,62,63] or Al [64,65] direction during DB and RB. However, it was not clarified which parameters influence the diffusion direction.

Regarding diffusion coefficients of Al in Ti and vice versa, findings in the literature are rare and controversial. Thiyaneshwaran et al. [54] performed DW of cp Al and Ti and found the diffusion of Al into Ti at 550 °C to be 20 times faster than vice versa. Bergner [66] calculated the diffusion coefficient of Ti in Al to be $3.8*10^{-18}$ m^2/s at 550 °C. Köppers et al. [67] investigated the diffusion of a pure Al layer evaporated on pure Ti and found the diffusion coefficient to be $1.6*10^{-21}$ m^2/s at 650 °C, while Räisänen et al. [68] calculated it to $1*10^{-19}$ m^2/s at 650 °C and $3.2*10^{-20}$ m^2/s at 600 °C by tracing ion-implanted Al atoms in Ti. Fig. 8 summarises the reported diffusion coefficients of Al/Ti. While the trend found for Ti in Al is reasonable for all investigations, indications for both the diffusion coefficient of Al in Ti being higher and lower as vice versa are found equally. At this point, it could not be clarified what causes these deviations in diffusion coefficients. When Ti6Al4V is used instead of pure Ti, the diffusion coefficient is found to be significantly lower [53]. This is reasonable, as the initial concentration gradient, which is the driving force for diffusion, is lower.

However, as mentioned before, dislocations and grain boundaries are inevitable for diffusion. Gachon et al. [52] found sputtering of layers to drastically increasing the number of grain boundaries and inter-grain boundaries and stated this to increase the diffusion rate up to 4 orders of magnitude. Plastic deformation of the Al alloy also increases the number of dislocations. This stimulates (dynamic) recrystallisation and the formation of sub-grain and grain boundaries, consequently, the diffusion rate is enhanced [16]. Robson [72] calculated the plastic deformation of Al to increase the diffusivity of Cu atoms by up to 5 orders of magnitude mainly due to the increased numbers of vacancies. This process of enhanced atomic migration along dislocations is schematically shown in Fig. 9: The aluminium undergoes severe plastic deformation (a), which introduces dislocations that are occupied by diffusing titanium atoms. Simultaneously, the material flow in deformation-driven processes moves diffusing elements and grain boundaries, so that, integrated over time, diffusion paths are found all over the interface region. Subsequently, the Ti atoms jump from dislocation to dislocation and diffuse deeply into the Al matrix (b). As the dislocations act as a “pipeline”, this process is described as “pipe diffusion” [73]. It allows for the formation of a noticeable diffusion layer even at the short processing times during FSW and similar processes [46,74,75]. If the Ti concentration increases further, $TiAl_3$-IMC precipitates form the diffusion layer (c). The same effect can be assumed for ultrasonic stimulation [76]. Furthermore, Li et al. [77] stated that the deformed interface itself after FSLW tends to reduce its free energy by reducing the surface. Consequently, interdiffusion is enhanced by the trend towards a flattened interface. Chen and Nakata [78] stated that for FSLJ the joining region is only within the diameter of the tool probe and therefore in the stir zone, which underlines the effect of plastic deformation. Xu et al. [60] measured the interlayer thickness during annealing of RB samples and found it to increase with increasing amount

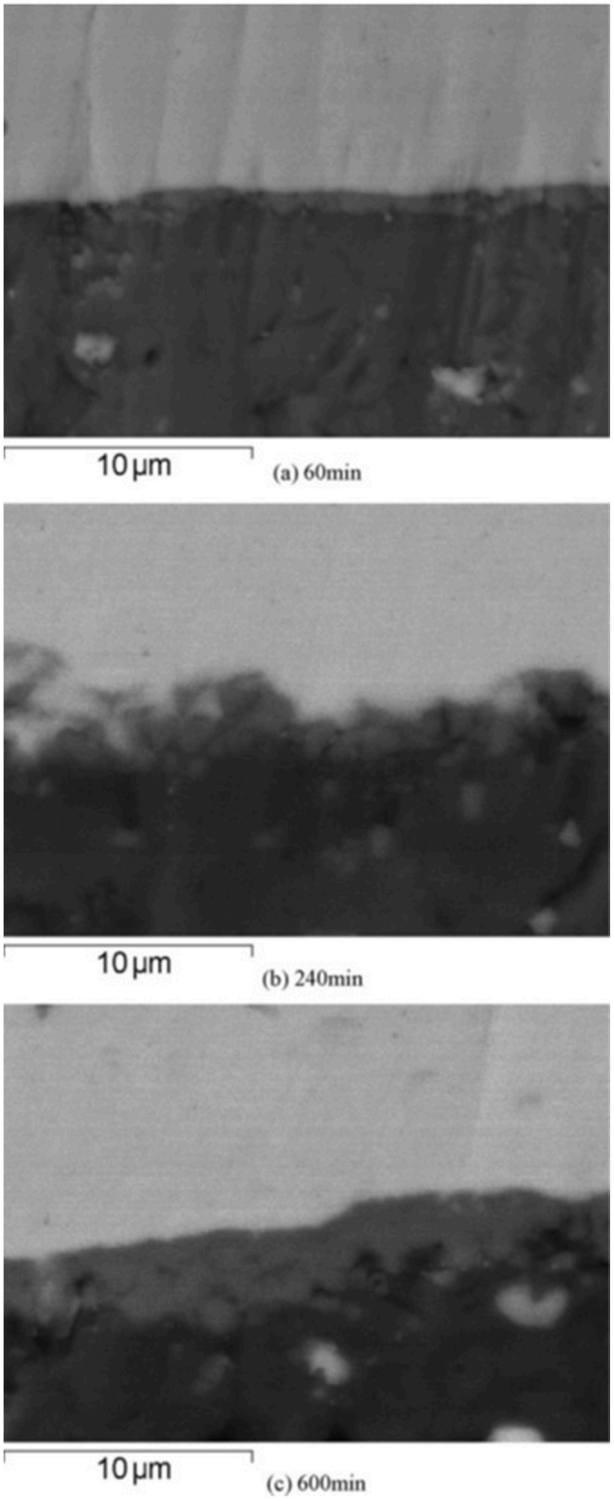

Fig. 7. Backscattered electron images of bonded joint under 650 °C and different times showing the evolution of IMC during DW, reprinted from Ref. [55] with permission from Elsevier.

of thickness reduction, i.e. plastic deformation. Furthermore, in deformation-based processes, diffusion is often found to be in the direction of Al [79]. Additionally, Yu et al. [22] stated that at high heat input during FSLW, also the Ti alloy is plastically deformed. This plastic deformation might also enhance the diffusivity of Al into Ti and boost joint formation.

After the formation of a continuous intermetallic layer, van Loo and Rieck [4] assumed diffusion through the IMC to be mainly by grain boundary diffusion because activation energy and frequency factor of the Arrhenius equation were found to be low. This is plausible as the microstructure within the IMC is found to be very fine-grained (1–5 µm) [60].

In summary, interdiffusion of Al and Ti becomes significant at temperatures around 520–550 °C. Additionally, several investigations show a time delay before diffusion. For the direction of interdiffusion, there are contradictory observations, which are so far not fully explained. Pressure and material flow can significantly enhance the diffusion rate and lower the diffusion start temperature, which allows for firm bonding at short times and lower temperatures during deformation-driven processes. It has been proven, that increasing plastic deformation enhances the diffusion rate within a material. Therefore, when Al is plastically deformed, it is reasonable to assume that the interlayer tends to grow in Al direction. Continuing diffusion leads to a saturation of Al in Ti or vice versa, which is a precondition for the precipitation of IMC as described in the following section.

5. Intermetallic compounds

Al and Ti are known to form a series of intermetallic phases. While some of them evolve from other phases (type–II– aluminides [26]), $TiAl_3$, TiAl and Ti_3Al are the only phases directly formed [80]. From these phases, $TiAl_3$ releases the highest amount of energy during formation, see Fig. 10, which is therefore formed primarily. The crystal structure of the $TiAl_3$-layer is determined as D022 [61]. The presence of TiAl and Ti_3Al after some processes is attributed to the stoichiometry in the interface between $TiAl_3$ and Ti. Choi et al. [43] found TiAl and subsequently Ti_3Al to form out of Ti and $TiAl_3$ during FSBW of pure Al and Ti when increasing the rotational speed. Increased energy input enlarges the number of diffused atoms as well as the diffusion distance. Higher Ti content before chemical reaction and a sufficient energy input promote the formation of Ti-rich phases. As seen in Fig. 10, the free energy of formation for TiAl and Ti_3Al is comparable in the temperature range around 500 °C, so both phases are likely to form.

With increasing processing temperature, the diffusion-controlled reaction between Al and Ti changes to a chemical-controlled reaction when the diffusion rate is higher than the reaction speed for the linear growth phase. Zhang et al. [81] identified the transition temperature to be between 550 and 575 °C in annealing of cp Al/cp Ti-sintered plates. Only when the growing $TiAl_3$ layer hinders the supply of Al, a slower parabolic behaviour begins and the growth conditions change back from chemical-controlled to diffusion-controlled [82]. While the Al–Ti reaction scheme (Fig. 11) expects the formation of IMC to take place only above 665 °C, several researchers have found mechanical stirring to reduce the start temperature significantly. The effect of strain-induced solid-state chemical reactions were studied and mathematically described in detail by Levitas et al. [83,84] for Ti–Si mixtures, representing a slightly different material system. Fronczek et al. [85] found the starting temperature for $TiAl_3$ formation in EW samples to be at 552 °C. For RB samples, it was observed at 550 °C during PWHT [75]. However, no explanation for the reduced reaction start temperature was provided. Zhang et al. [81] calculated FSP of cp Al/cp Ti-sintered plates to stimulate the Al–Ti-reaction similar to annealing at 710 °C, which is around 100 K more than the FSP process temperature. The reaction rate constant was found to be around 6 times higher than of annealing at 650 °C. This was attributed to two effects: First the Ti particles were refined and therefore the reaction surface enlarged, as well as the reaction product was dispersed, second the atoms were activated by severe plastic deformation. Van Loo and Rieck [4] found $TiAl_3$ to form during DB of TiAl and pure Al already at 516 °C. As no other phase appeared or grew, they concluded that during diffusion experiments below 640 °C only $TiAl_3$ forms. Additionally, the IMC showed two lattice modifications. Besides the well-known hexagonal $TiAl_3$, here called “high--temperature” (formed at all investigated temperatures), a second

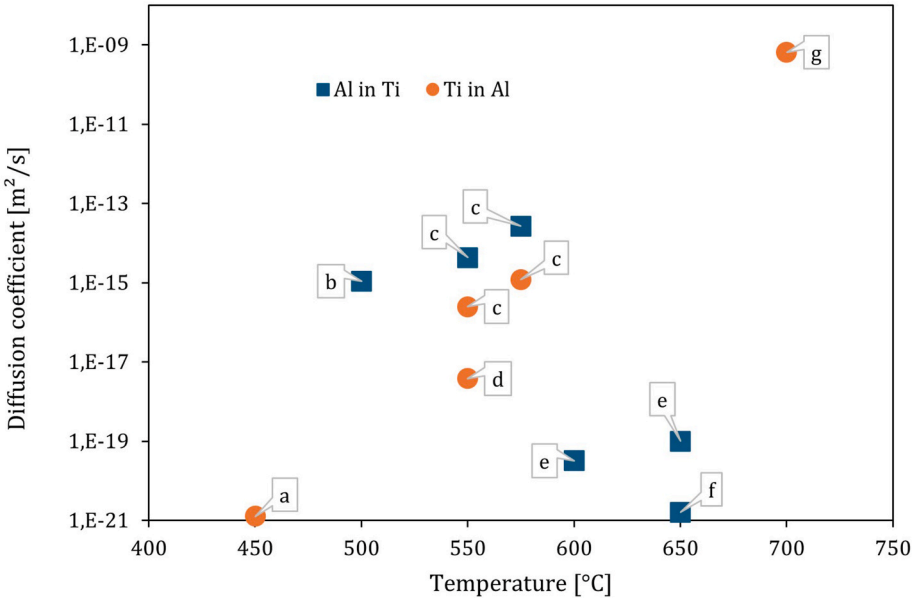

Fig. 8. Diffusion coefficient (m^2/s) in DB of Al in Ti and vice versa (values taken from a [69]; b [70]; c [54]; d [66]; e [68]; f [67]; g [71]), showing significant variation for diffusion of Al in Ti.

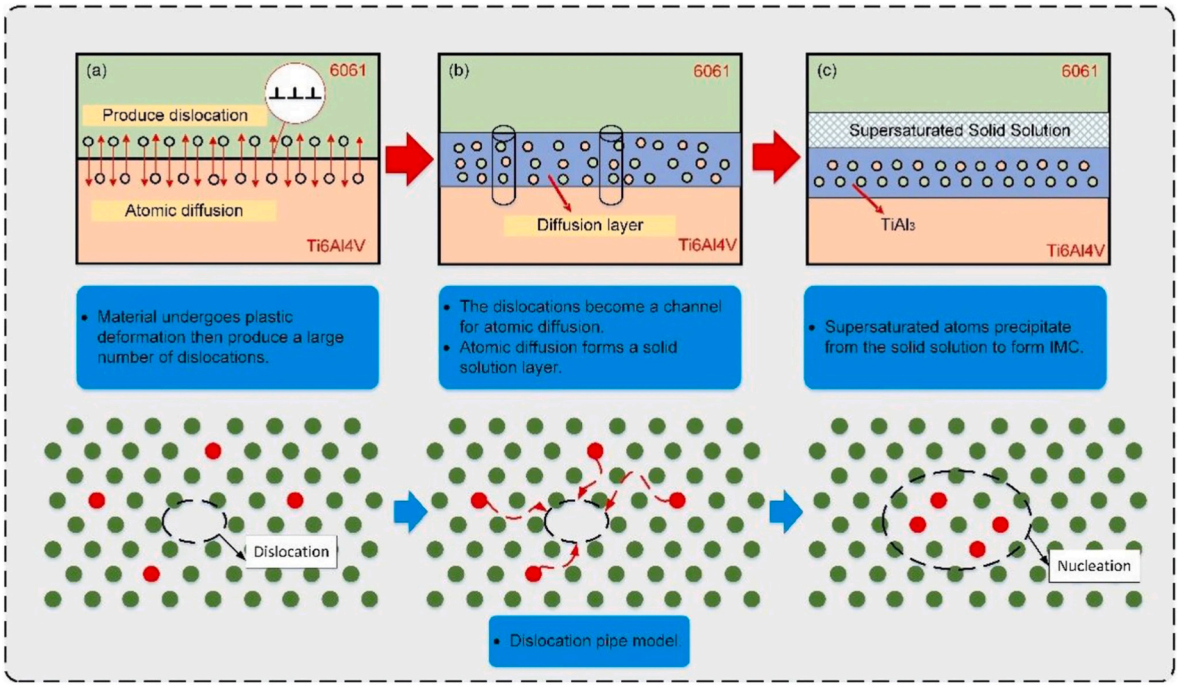

Fig. 9. Schematic of interface formation in deformation-based joining of Al and Ti showing: a) introduction of dislocations due to plastic deformation of Al, b) diffusion of atoms along the dislocation "pipelines" and formation of a solid solution layer and c) nucleation of IMC from the supersaturated solid solution, reprinted from Ref. [73] with permission from Springer Nature.

modification, called "low-temperature" (formed only around 585 °C), is observed. Here, the latter one was described as super-structure (Ti_8Al_{24}) due to the fourfold c-axis [4].

Regarding the growth behaviour of the IMC in DB over time, no generally accepted description is provided in literature. Fuji [86] described two steps during PWHT of FW samples: Nucleation of IMC and coarsening of the nuclei. The second step is characterised by a roughly linear growth of the layer, see Fig. 12, and its relatively slow kinetics is assumed to be caused by thin oxide films on Ti [4]. Plaine et al. [87] and Kar et al. [88] made similar observations but described the first step as the 'incubation period'. While Plaine et al. [87] reported the incubation period as 3 s during welding, Kar et al. [88] found an incubation period to occur during PWHT, especially at temperatures below 600 °C. At longer PWHT times, latter observed a third step of parabolic or asymptotic growth towards complete consumption of the Al-layer. As the formation of $TiAl_3$ is exothermic, the reaction could even cause local melting of Al [89]. During the transition between the second and the third step, a band of pores is observed near the Al-IMC interface. These pores are believed to be Al inclusions, covered by Al oxides, that are dissolved after being entrapped by the IMC [4]. For FSBW of Al and

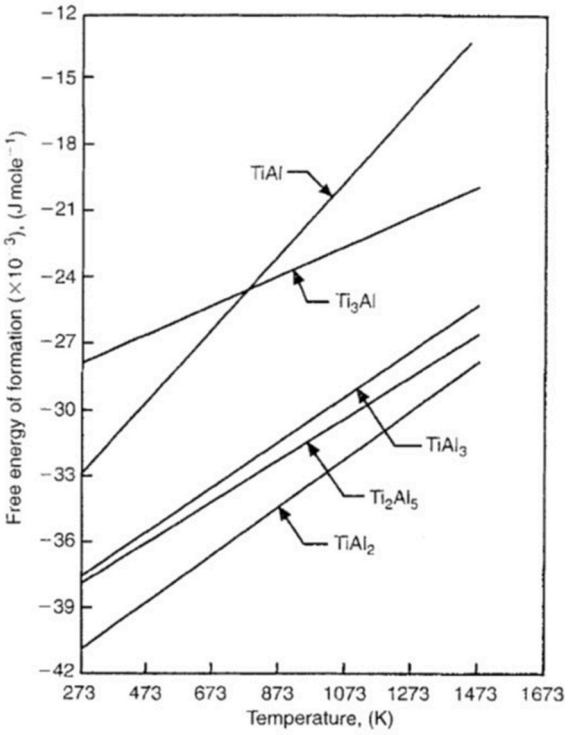

Fig. 10. Calculated Gibbs free energies of formation of different Ti–Al compounds as a function of temperature, reprinted from Ref. [26] with permission from Springer Nature.

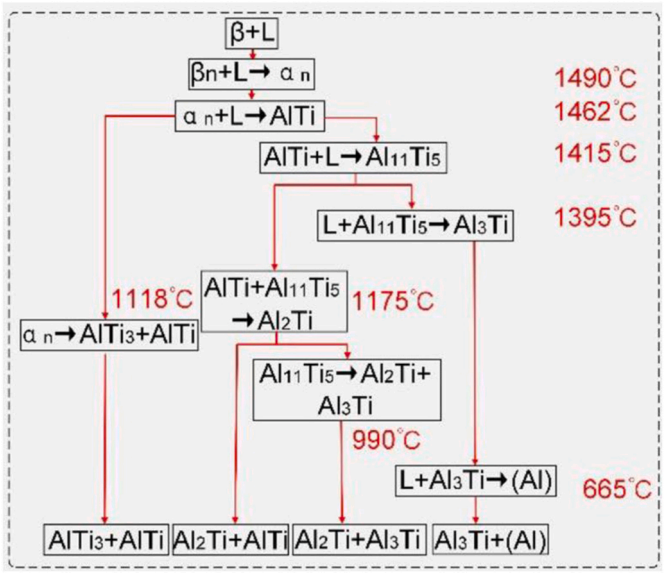

Fig. 11. Intermetallic reaction scheme for Al and Ti showing transition temperatures and evolving phases during cooling from the liquid state, reprinted from Ref. [73] with permission from Springer Nature.

steel, Tanaka et al. [90] found similar growth behaviour. They observed the first step (nucleation) to occur around the tool probe especially due to plastic deformation and mechanical mixing while the second one (linear stage) below the shoulder is due to the frictional heat.

Growth of an already existing layer is found to start at lower temperatures. Leo et al. [91] detected growth of the $TiAl_3$ layer and evolution of a new TiAl phase to occur already during PWHT at 450 °C for 138 h in laser-welded samples. Moradi et al. [92] found the reaction-start-temperature for $TiAl_3$ growth to be decreased to even 425 °C after accumulative RB. During PWHT, the reaction rate increases from ~5 μm/50 h at 550 °C to ~200 μm/50 h at 630 °C, as shown in Fig. 13. This is confirmed by other investigations like laser weld-brazing [93]. As the layer growth rate is almost linear over time, Zhang et al. [94] concluded that the diffusion coefficient in the $TiAl_3$ layer is comparable to that in the base materials.

After nucleation of the IMC, most researchers found the layer to grow in the direction of Al, driven by two effects: First, the chemical composition requires two times more Al. Hence, considering almost equal diffusivity through the existing layer, the stoichiometry at the Al–$TiAl_3$-interface is advantageous. Second, the solubility of Al in Ti is 100 times higher than vice versa, so that a saturated solution is reached much earlier [60]. However, Fuji [86] found the intermetallic layer to grow in the direction of Ti during PWHT of FW pure Al–Ti samples, but did not deliver an explanation for this observation.

The above-mentioned effects occur during thermo-mechanical processing of mainly the Al substrate. If also Ti is subjected to severe plastic deformation, the type of IMC formed changes. Kar et al. [88] used FSBW to join two cp Al sheets with an 1 mm cp Ti interlayer and found mainly the formation of $TiAl_2$ and Ti_2Al_5, which are normally considered as type–II–aluminides. During PWHT, they observed the formation of $TiAl_3$ and the dissolution of the previous compounds above 600 °C. For the same process using AA6061 on the Al-side, Sundar et al. [95] detected two distinct layers, namely Ti_2Al_5 (on the Ti-side) and $TiAl_3$ (on the Al-side) in the interface. This indicates that mechanical mixing does not only accelerate the reaction between Al and Ti but also changes the reaction mechanisms so that type–II–aluminides are directly formed, or type-I-aluminides are directly converted. However, as described later, it must be noted that the process temperatures during the plastic deformation of Ti are also significantly higher and partially above the Al solidus temperature.

In general, $TiAl_3$ is the most frequently found IMC in SSSJ of Al and Ti. However, other, Ti-rich phases can precipitate at the interface between Ti and $TiAl_3$. For sufficient long process times, $TiAl_3$ is formed out of all other Al–Ti-IMC. Formation of IMC is either controlled by the diffusion rate (supply of atoms) or the reaction speed (dissipation of free energy). Plastic deformation reduces the starting temperature for the Ti–Al-reaction from 665 °C to about 550 °C and the temperature required for layer growth to ~425 °C. Growth of IMC does not follow a continuous function but occurs in three steps: Incubation period, linear growth stage and asymptotic growth. In the following section, the influence of the formation of IMC on the mechanical properties is discussed.

6. Mechanical properties

Mechanical strength of dissimilar Al–Ti joints depends on two factors: The strength of the Al–Ti interface and the strength of the thermal or thermo-mechanical affected Al. As the focus of this review is on the joining of Al and Ti, the thermally induced deterioration of Al will not be analysed in the following section. The interested reader is referred to a comprehensive review of mechanical properties in SSSJ of Al and Ti published by Gadakh et al. [13].

Over all investigations, quasi-static mechanical properties (i.e. ultimate tensile strength (UTS) and LSS) are mainly investigated. Dynamic mechanical properties are scarcely investigated, so that general conclusions cannot yet be drawn. However, Plaine et al. [96] found the fatigue strength of AA5754-Ti6Al4V joints to be 25 MPa, 15 % of the static LSS, while Yazdanian et al. [97] have found tool diameter and cp Al interlayer to have almost no effect on fatigue strength in FSLJ of AA2024 and Ti6Al4V.

Maximum joint efficiencies (ratio of weld UTS to Al base-metal UTS) reached in SSSJ of Al and Ti are in the range of 70–100 %. For example, Wei et al. [98] achieved 100 % efficiency in FSLW of AA1060 to Ti6Al4V using a cutting probe to scratch the Ti surface. Kimura et al. [99]

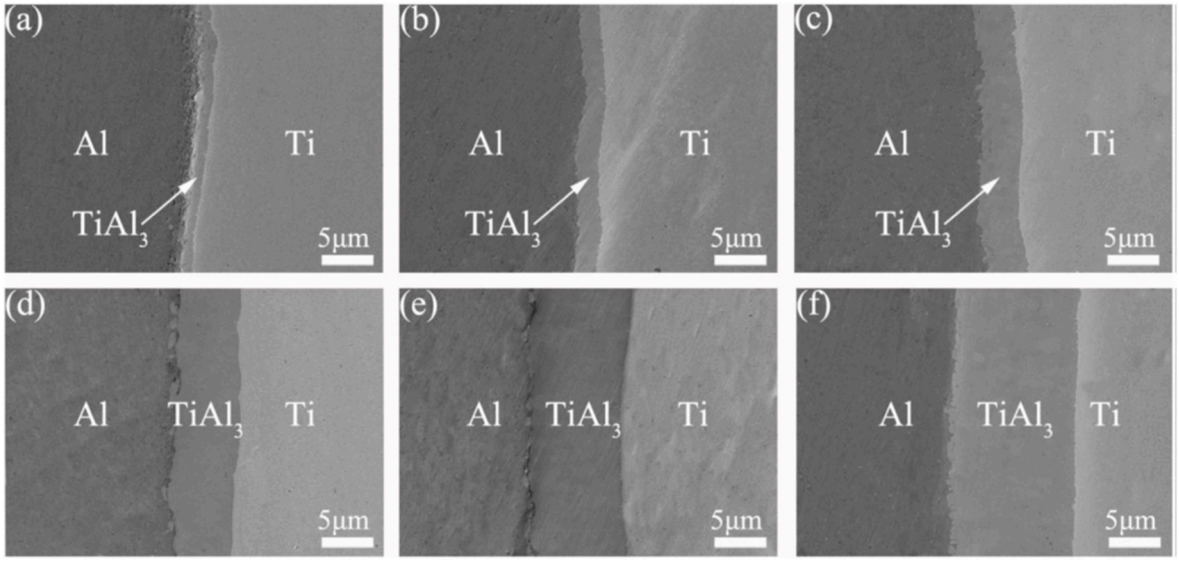

Fig. 12. Interface micrographs of Al6061/Ti6Al4V hot RB sheets after annealing at 600 °C for (a) 1 h, (b) 2 h, (c) 4 h, (d) 8 h, (e) 12 h and (f) 16 h, reprinted from Ref. [75] with permission from Elsevier.

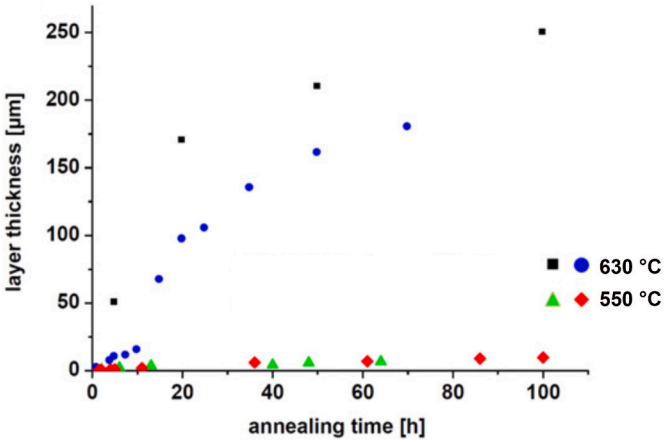

Fig. 13. Average $TiAl_3$ layer thickness of annealed samples at 550 °C and 630 °C, adapted from Ref. [85] with permission from Elsevier.

obtained a joint efficiency of ~100 % during FW of AA5052 to Ti6Al4V, while Rostami et al. [100] reached 94 % in FSBW for the same combination. Ma et al. [101] realized 85 % of joint efficiency during ultrasonic-assisted FSBW, Bang et al. [102] 91 % during gas tungsten arc welding assisted FSBW and Li et al. [77] 95.5 % by FSLW and PWHT of A6061 to Ti6Al4V. For joints of AA2024 to Ti6Al4V, Dressler et al. [42] measured 73 % as the limit in FSBW. Plaine et al. [103] achieved for AA5754 to Ti6Al4V refill FSSW lap joints a maximum lap-shear force of almost 7000 N,[1] clearly above the AWS D17.2/D17.2 M standard of 4270 N. On AA6181 to Ti6Al4V, the maximum lap-shear force was approximately 6500 N [104]. However, a broad range of investigations reported also significantly lower maximum strength [59,78,105].

Kim and Fuji [15] were the first that investigated the influence of the intermetallic layer thickness on the mechanical properties of FW and PWHT samples systematically. They found the thickness of the IMC layer to be the most significant influence in terms of mechanical properties. During PWHT, the tensile strength decreased drastically, when the thickness of the $TiAl_3$ layer exceeded 5 µm (see Fig. 14 @10–30 h), representing the critical value before embrittlement and therefore deterioration of tensile strength. Further mechanical factors, i.e. residual stresses, were stated to be negligible.

The influence of other types of IMC is scarcely investigated. Zhang et al. [106] used molecular dynamics modelling to simulate the maximum interface strength of Al/$TiAl_3$/Ti and Al/$Ti_2Al_{18}Mg_3$/Ti combinations and found them to be 8000 N/mm^2 and 2500 N/mm^2, respectively. Furthermore, they calculated the fracture to occur in the Al/$TiAl_3$-interface for the first case but in the other case within the $Ti_2Al_{18}Mg_3$.

In contrast to Kim and Fuji, Rajakumar and Balasubramanian [59] found for DB of AA7075 and cp Ti that a copper-containing intermetallic layer ($AlCu_2Ti$) of 7 µm resulted in maximum lap-shear strength (LSS). However, the maximum LSS of approximately 80 MPa (~15 % of base metal) was relatively low compared to other investigations. Assuming

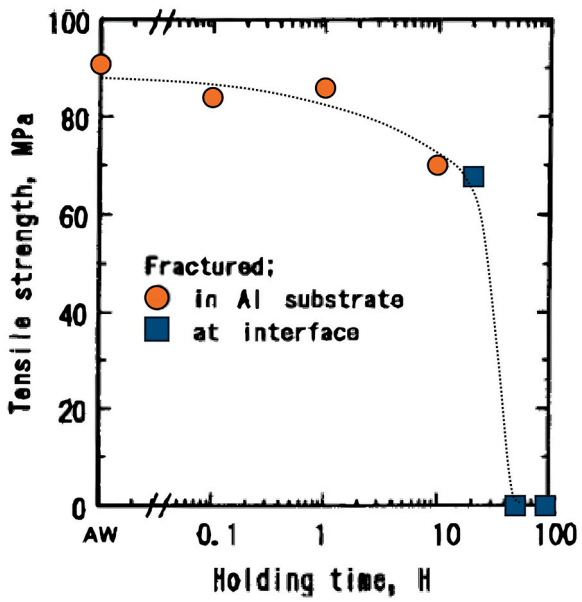

Fig. 14. Tensile strength of FW Al–Ti-samples over PWHT time at 600C, adapted from Ref. [15] with permission from Sage Publications.

[1] Since the bonded surface is usually not precisely known in refill FSSW, usually only the maximum lap-shear force is specified.

similarities of Al–Ti to Al-steel joining, it is relevant to mention that Beygi et al. [107] reported triaxial stresses generated around the IMC during tensile loading for Al-steel. These are caused by differing modulus of elasticity between base metals and IMC. Triaxiality increases with the thickness and continuity of the IMC as well as increasing interface roughness. Consequently, this might causes brittle failure [23]. Lee et al. [108] investigated PWHT of RB cp Al–Ti and found the highest peeling strength, if an area fraction of 75–80 % of $TiAl_3$ remained on the Ti surface. Lower time-temperature regimes led to lower bonding area while higher energy led to an embrittlement when the IMC covers more than 80 % of the surface and its thickness exceeds 300 nm.

In contrast, directly after welding, studies like Li et al. [109] (FSBW of AlMg6 to Ti6Al4V) found highest tensile strength if only diffusion and no IMC was present as the latter contained micro cracks. Furthermore, Dressler et al. [42] found the fracture to propagate partially through the interface and the Al. They concluded that in regions where Al was still bonded to Ti, a chemical bonding (i.e. IMC) was present and acted as an adhesion-promoting agent. Esmaeili et al. [110] reviewed characteristics of intermetallic compounds in several dissimilar FSW combinations and found uniformity, continuity and low thickness necessary for highest mechanical properties.

For DB of pure Al and Ti, Wei et al. [55] described the evolution of joint strength over time as follows: First, joint strength increases proportionally to the thickness of the interdiffusion area (region a in Fig. 15). With the first appearance of IMCs, the bonding between IMC and diffusion area is not as firm and homogeneous, so the slope of joint strength over time is reduced (region b in Fig. 15) until a layer is formed and joint strength increases rapidly until it exceeds the strength of the base Al (region c in Fig. 15).

Especially during FSBW, Ti fragments are dispersed in the Al matrix. While some researchers believed them to have a particle-strengthening effect [59,111], others like Choi et al. [43] found them to cause defects near the weld interface that reduce the mechanical properties. Additionally, during mechanical loading, they act as crack initiators due to the significant difference in Young's modulus compared to the Al base material.

The previously mentioned results are summarised in Table 2. As outlined, SSSJ-techniques are under certain conditions able to produce joints with properties close to the base material strength. Thin IMC formation can be seen as an indicator for significant previous diffusion and therefore firm bonding, however, intensive growth over a few micrometres thickness embrittles the joint. Controlling the interface reaction by the energy input, as described subsequently, is necessary to achieve good bonding and high joint ductility simultaneously.

7. Energy input

Energy input plays a crucial role in formation of IMCs between Al and Ti. Because of the differing thermal properties of Al and Ti, joining temperatures have to be close to the solidus temperature of Al. Therefore, the process parameter window between incomplete bonding and overheating of Al is relatively narrow [120]. Energy is provided either by heat (DB, laser/arc welding) or friction (FW, FSW, refill FSSW, UW). Mechanical impact is comparatively more effective as it induces also dislocations [73] and breaks up oxide layers [56]. Kalinenko et al. [47] described the bonding mechanisms in FSLJ to be close to DB but enhanced by large plastic deformation. Li et al. [109] reported the surface of the Ti to be activated by the rubbing motion of the tool. For refill FSSW, Plaine et al. [121] found a thin and discontinuous intermetallic compound layer in the shoulder region of AA6181-T4 to Ti6Al4V joints, while the layer was significantly more pronounced in the probe region. This might be a result of the 20 K higher temperature in the probe region. Varying the depth of penetration into the Ti alloy in FSBW, researchers like Wu et al. [115,116] found no acceptable joint to be formed without penetration but a decrease in required energy input and increase in process parameter window when the penetration was increased to ~ 1 mm. On the other hand, for FSLJ, researchers like Kalinenko et al. [47] and Krutzlinger et al. [122] also found increasing tool to interface distance detrimental for joint strength, while the maximum joint strength is reached as the tool is touching but not penetrating the Ti [113]. In this case, Krutzlinger et al. [122] reported plastic deformation on the Ti surface by the Al material flow. Krutzlinger et al. [122] and Wu et al. [115] also found the rotation speed and therefore the maximum process temperature to be the key factor determining joint properties. Comparing conventional and stationary shoulder FSBW, Sundar et al. [123] found $TiAl_3$ to form in conventional FSBW, while a thinner layer consisting of Ti_2Al_5 was detected in stationary shoulder FSBW, which was attributed to the decreased heat-input. For EW, Liang et al. [124] calculated that a direct joining of AA7075 and Ti6Al4V is not feasible due to the low melting point and high strength of AA7075 as there is no weldability window between the limiting factors in EW, namely formation of a material jet, excessive melting, the weld shape and the acoustic velocity.

In contrast to other investigations, Buffa et al. [119] used Ti as the top sheet in FSLW to AA2024 and consequently found the lowest heat input to be beneficial for joint strength. However, joint efficiency of only 10 % could be reached.

To address the discrepancy between sufficient heat input and overheating of the Al alloy, some approaches were tried to restore or preserve the Al properties. Kar et al. [112,125] suggested two-pass FSBW,

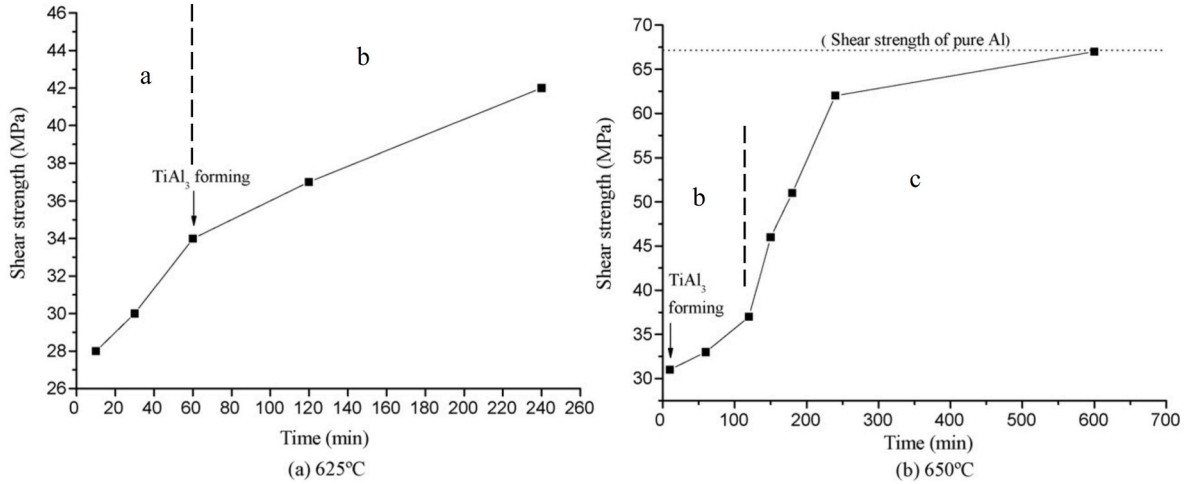

Fig. 15. Joint strength of pure Al–Ti-joints in DB over time, adapted from Ref. [55] with permission from Elsevier.

Table 2
Overview on influence of Al alloys, energy input and SSSJ processes on mechanical properties.

ALLOY SYSTEM	PROCESS	MECHANICAL PROPERTIES	FURTHER OBSERVATION
cp Al/cp Ti	FW and PWHT	100 % joint efficiency 90 MPa UTS [15]	– Tensile strength decreased drastically, when the thickness of the IMC layer exceeded 5 µm.
	Two-pass FSBW	133 % joint efficiency 92 MPa UTS [112]	– UTS increased by 27 % due to second pass.
AA1060/ Ti6Al4V	FSLW with cutting probe	100 % joint efficiency 63 MPa LSS [98]	
AA2024/ Ti6Al4V	FSBW	73 % joint efficiency 348 MPa UTS [42]	– Fracture propagated partially through the interface and the Al. – IMC acted as an adhesion-promoting agent.
AA5052/ Ti6Al4V	FW	100 % joint efficiency 194 MPa UTS [99]	
	FSBW	94 % joint efficiency 258 MPa UTS [100]	
AA5754/ Ti6Al4V	refill FSSW	lap-shear force 7000 N (110 MPa LSS[a]) [103]	
AlMg6/ Ti6Al4V	FSBW	93 % joint efficiency 292 MPa UTS [109]	– Highest tensile strength if only diffusion and no IMC was present. – Ti surface activated by rubbing motion of tool.
AA6060/ Ti6Al4V	FSLJ	70 % joint efficiency (112 MPa LSS[a]) [113]	– Maximum joint strength as the tool is touching but not penetrating Ti.
AA6061/ cp Ti	Water-cooled FSBW	42 % joint efficiency 120 MPa UTS [114]	– Water cooling increases UTS by 20 %.
AA6061/ Ti6Al4V	ultrasonic-assisted FSBW	85 % joint efficiency 236 MPa UTS [101]	
	gas tungsten arc welding assisted FSBW	91 % joint efficiency 300 MPa UTS [102]	– Pre-heating of Ti increased UTS by 24 %.
	FSBW	68 % joint efficiency 215 MPa UTS [115, 116]	– No acceptable joint without penetration of Ti. – Decrease in required energy input and increase in process parameter window when the penetration was increased to ~1 mm.
AA6181/ Ti6Al4V	refill FSSW	lap-shear force 6500 N (102 MPa LSS[a]) [104]	
AA7050/ Ti6Al4V	FSLJ	34 % joint efficiency (63,5 MPa LSS[a]) [117]	– Interface temperature reaches up to 570 °C.
AA7075/ cp Ti	DB	15 % joint efficiency 80 MPa LSS [59]	– Copper-containing intermetallic layer (AlCu2Ti) of 7 µm resulted in maximum LSS.
AA7075/ Ti6Al4V	FSBW and artificial ageing	83 % joint efficiency 505 MPa UTS [118]	– improvement in joint strength by 15 %.
Ti6Al4V/ AA2024	FSLW	10 % joint efficiency[(44 MPa LSS[a]) [119]	– Lowest heat input beneficial for joint strength.

[a] Values estimated from reported bonding area.

where the first pass thermo-mechanically affects the Ti while the second one homogenises especially the Al microstructure and breaks up Ti particles. Therefore, the joint strength could be increased by 27 %. Similar results were obtained by Österreicher et al. [118] for FSBW of AA7075 and Ti6Al4V by using artificial ageing. The improvement in joint strength by 15 % is explained by reprecipitation in the Al microstructure. Bang et al. [102] used gas tungsten arc pre-heating for the Ti6Al4V plate in FSBW to reduce the necessary heat input on the AA6061-side, which ensures a homogeneous weld interface. This resulted in a 24 % improvement of the joint strength. In contrast, Patel et al. [114] investigated heating and cooling during FSBW of AA6061 and cp Ti and found water cooling to increase the tensile strength by 20 %. Zhang et al. [126] introduces a stepped interface in FSBW of AA2024 and Ti to increase the deformed volume of Ti in the root section of the weld and therefore homogenise the heat distribution. This led to up to 18 % increase in joint UTS.

Regarding the risk of overheating, determining the actual interface temperature in deformation-based processes is relatively challenging as Al is in general plastically deformed and the thermal conductivity of Ti is quite poor. Usually, the peak interface temperature is believed to be below the solidus temperature of the Al alloy [127], which seems to be valid if the tool is only in contact with the Al alloy, like in refill FSSW [73,103,128]. However, if the Ti is scratched or plastically deformed (like in FSBW), the temperature in the interface between the tool, Al and Ti will most likely surpass this point. Sundar et al. [129] measured the temperature evolution in Al during FSBW at 15; 20 and 25 mm from the interface, see Fig. 16. They estimated the peak temperature in the interface by linear extrapolation to be above 600 °C (20 K above the solidus temperature), when the probe was inserted into the Ti6Al4V by approximately 2 mm during FSBW with AA6061. Similar results were found by the authors of this work [117] for FSLJ of AA7050 to Ti6Al4V, where the interface temperature was directly measured by thermocouples embedded in the Ti at the interface. Here the temperature at the contact point of Ti and the tool exceeded the solidus temperature by 80 K and reached up to 570 °C, see Fig. 17. Also for UW, the interface temperature reaches the Al solidus as measured by Zhang et al. [130] for AA1060 and cp Ti.

In summary, SSSJ of Al and Ti is performed close to the Al solidus temperature. As plastic deformation enhances the reaction, temperature and process time can be reduced. Most effective joining is reached as the Ti surface is slightly plastically deformed. For process apart from DB and PWHT the maximum process temperature is determined as the most effecting energetic parameter. However, the actual interface temperatures are often not known, so that partial melting of Al cannot be ruled out. To restore or preserve the Al properties, several approaches like cooling or PWHT are applied.

8. Influence of alloying elements

Diffusion and accumulation of several alloying elements such as silicon, copper and magnesium in the interface were observed by several researchers [56,61,131,132]. Both are present especially in DB and PWHT, while shorter process times and material mixing in deformation-based processes hinder accumulation. Elemental accumulation is believed to be caused by different diffusion rates and affinities towards Al and Ti [46]. A first comparative review on the influence of alloying elements for Al and steel has been published by Beygi et al. [23]. To the best of the authors' knowledge, there is no systematic investigation for SSSJ of Al and Ti. Besides the diffusion, alloying elements also have a significant influence on the formation of IMCs. Takemoto and Okamoto [133] analysed brazing of Ti with Al filler materials and found the addition of alloying elements to liquid Al to slow down the kinetics of $TiAl_3$ formation. Furthermore, the

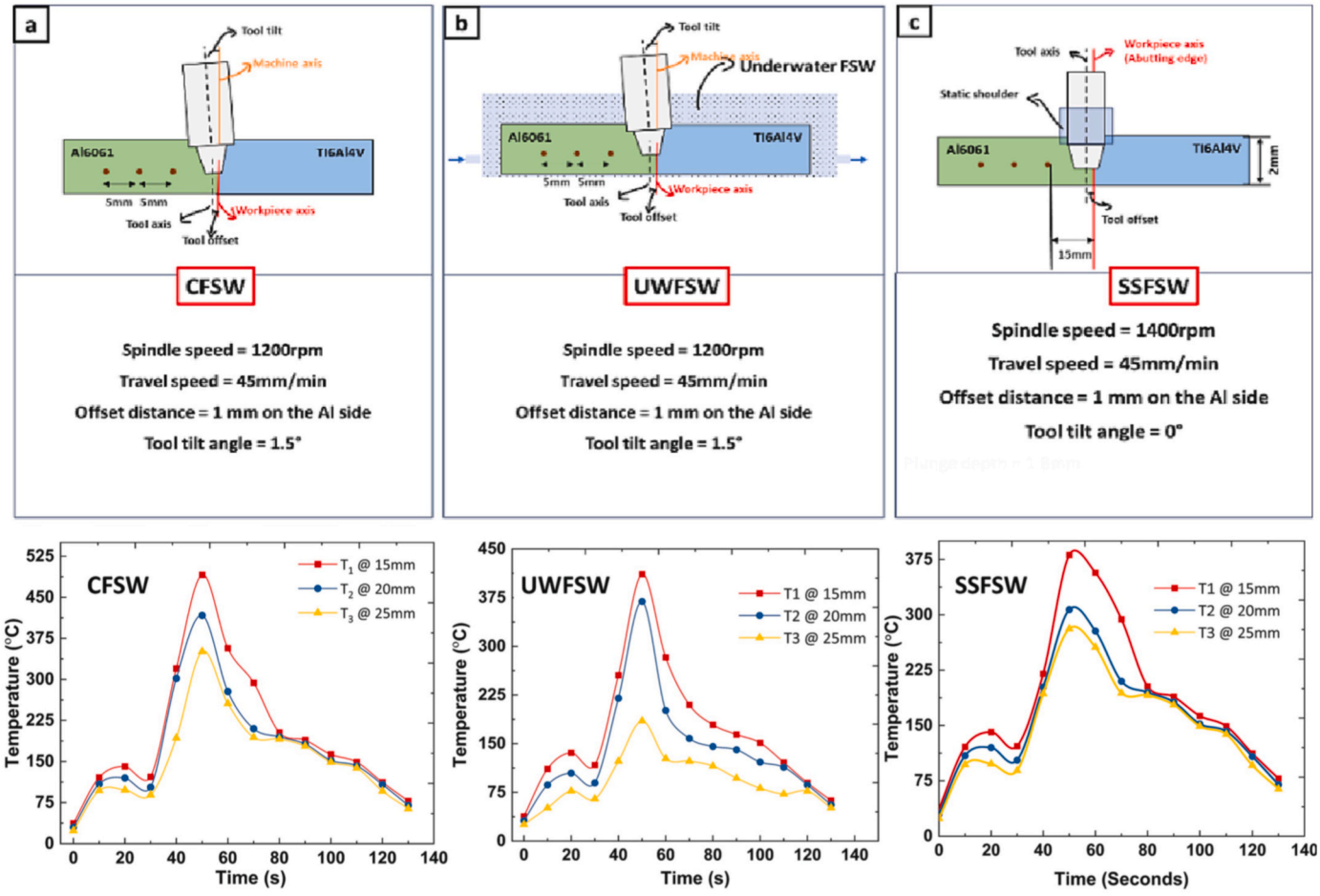

Fig. 16. Measured time-temperature evolution in the aluminium close to the welding interface in three modifications of FSBW: a) conventional FSBW, b) underwater FSBW, c) stationary shoulder FSBW, adapted from Ref. [129] with permission from Elsevier.

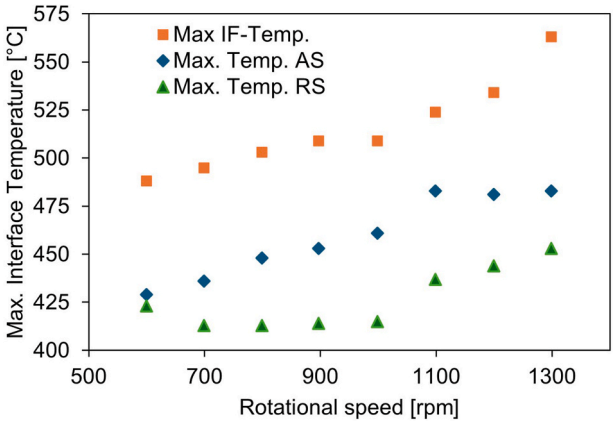

Fig. 17. Maximum interface temperatures measured during FSLJ of AA7050 and Ti6Al4V in the interface at the weld centreline and 5 mm on advancing and retreating side over rotational speed. Temperatures exceed the solidus of AA7050 (490 °C) significantly, reprinted from Ref. [117].

interdiffusion might also be influenced by the formation of local eutectics. Brown and Ashby [134] found the diffusion rate to be inversely dependent on the local melting temperature. Therefore, in phases with low solidus temperature the diffusion rate is higher and IMC with compositions close to the eutectic point are preferentially formed [23]. As the IMC might therefore not only consist of $TiAl_3$, the properties might be notably different [50].

Additionally, concerning deformation-based processes, alloying elements change the thermo-mechanical properties of the base materials and therefore influence the manner of energy. Because of the high ductility and solidus temperature as well as the low tensile strength of pure Al, joining with Ti is comparably simple to achieve [98,135], which is not the case for different (technologically relevant) Al alloys. The influence of relevant individual alloying elements is discussed in the following.

8.1. Aluminium

Although aluminium is one of the reaction partners, its concentration in the Ti alloy before joining also influences the reaction process. Van Loo and Rieck [4] found Al in Ti to cause a longer and faster linear growth stage of the IMC before the subsequent parabolic growth behaviour begins. Comparing FSBW of AA2024 and AA7075 to cp Ti and Ti6Al4V, Aonuma and Nakata [136] found the joint strength to Ti6Al4 to be generally lower. This might be due to the reduced concentration gradient caused by 6 wt% of Al on the Ti side, or the higher amount of V in the IMC.

8.2. Vanadium

Liu et al. [61] found vanadium to accumulate in the $TiAl_3$ phase at annealing temperatures of 500–650 °C and annealing times of 24 h, see Fig. 18. They concluded a combination of Si, V and Mg to retard the IMC formation because of the consumption of enthalpy and decrease of crystal defects. In contrast, Wang et al. [75] detected a constant amount

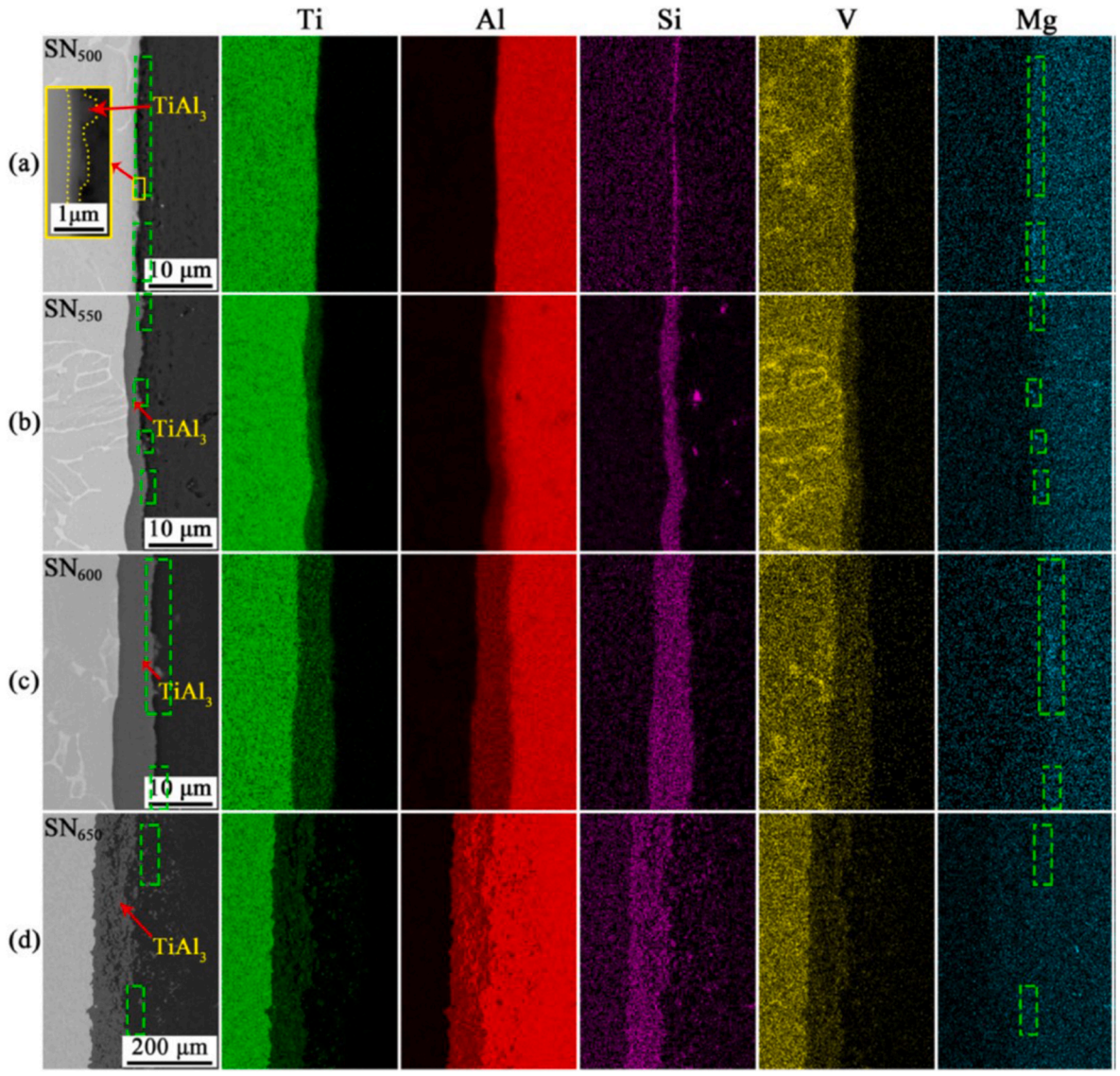

Fig. 18. Microstructure and EDS mapping analysis results of the Al/Ti interface after different annealing treatments at: (a) 500 °C−24 h (high magnification image in inset); (b) 550 °C–24 h; (c) 600 °C–24 h; (d) 650 °C–24 h (Zones with a slight Mg enrichment are marked in green dotted rectangles.) Reprinted from Ref. [61] with permission from Elsevier.

of vanadium in the IMC.

8.3. Copper

For DB of Al and steel, Yousaf et al. [137] reported copper to decrease the thickness of the IMC by up to 75 % for 11 wt% of Cu addition to Al, due to the formation of tetragonal intermetallic Al_2Cu and Al_7Cu_2Fe phases above 650 °C which consume the diffusing Al atoms. Similar effects can be assumed for Al and Ti. Tardy and Tu [138] added 0.25 at.% copper to Al which retarded the growth of the intermetallic layer as it increased the activation energy for Ti diffusion. In FSBW of AA6061 with Ti6Al4V, Mustafa et al. [139] found a 0.2 mm pure Cu foil to enhance the mechanical properties by mitigating the $TiAl_3$ formation. According to Malikov et al. [131], Cu accumulates in the $TiAl_3$ layer and adsorbs the diffusing Al and Ti atoms so that diffusion and thereby growth of the IMC is retarded. Kar et al. [140] investigated FSBW of cp Al and Ti using a copper interlayer and stated that Cu reduces the formation of $TiAl_3$. Instead, less brittle Al_aCu_b [141] and Cu_cTi_d-phases [142] are formed that absorb the diffusing atoms and might act as adhesion-promoting intermediate layers.

On the other hand, Cu–Al-eutectics decrease the solidus temperature of Al by around 150 °C [125], so that overheating and partial melting during the process is more likely to occur. Kar et al. [125] stated that the initiation temperature for IMC formation during DB (550 °C) cannot be reached in solid-state joining of Ti to Al–Cu-alloys and deformation-enhanced diffusion due to FSW or UW is crucial to achieve reliable bonding. Therefore, no investigation on DB of Al–Cu to Ti is known to the best of the authors knowledge. Additionally, for FSBW of Al–Cu-alloys to Ti, Dressler et al. [42] reported the necessary heat input to cause significant deterioration of the Al alloy. Consequently, attempts to reduce the peak temperature in Al are applied, like low rotation rates [143], under-water FSW [144], double-pass-FSW [125], and smaller shoulder diameters [105]. In contrast, Zhang et al. [145] found the maximum temperature in FSBW of AA2024 and TC4 plates to be 550 °C and therefore above the solidus temperature, so that semi-solid-state joining occurred, as the hot Ti contacts the Al directly behind the tool probe. Caused by the comparatively low process temperatures, deformation-based joining of Al–Cu-alloys to Ti without formation of IMC is likely to occur [146].

As Al–Cu alloys belong to the high-strength Al alloys, the joint

efficiency is typically comparably low (50 % [105] to 60 % [147]).

8.4. Manganese

Fuji et al. [148] found no significant influence of Mn addition on the interface formation during PWHT of FW samples. On the other hand, Kalinenko et al. [47] noticed increased concentration in the interface after FSLJ. Meisnar et al. [149] found Mn enrichments to alternate with Ti in the diffusion-type interface of FW AA6082 to Ti6Al4V, see Fig. 19.

8.5. Silicon

Silicon tends to be concentrated in the weld interface even directly after FSW [56] and UW [132], see Fig. 20. As the Si concentration in the interface was above the solubility maximum, Zhang et al. [132] concluded Si to either form precipitates or IMC, even if no Al–Ti IMC was detectible. Liu et al. [61] found silicon to be enriched in the IMC at annealing temperatures of 500–650 °C and annealing times of 24 h, see Fig. 18. By having a similar atomic radius, silicon replaces Al in the IMC up to 15 % [150] and forms $Ti(Al,Si)_3$ as well as Ti_5Si_3 [61] and $Ti_7Al_5Si_{12}$ [151]. Fuji [86] compared PWHT of FW samples of highly pure and commercially pure Al to Ti and found Si to hinder the diffusion of Al towards Ti and therefore the interlayer growth. This is in accordance with findings by Liu et al. [61] that a combination of Si, V and Mg retards the IMC formation because of the consumption of enthalpy and decrease of crystal defects. Comparing DB of Al–Mg (5056) and Al–Mg–Si (6013) alloys, Wilden and Bergmann [53] found the minimum diffusion temperature for AA6013 to be ~40 K higher, see Fig. 21, which is explained by the inhibiting effect of Si on the diffusion.

8.6. Magnesium

Liu et al. [61] found magnesium to accumulate at the interface between $TiAl_3$ and Al at annealing temperatures of 500–650 °C and annealing times of 24 h, see Fig. 18. With increasing temperature, Mg diffused into the IMC and the concentration at the boundary to Al decreased. While other researchers found no specific trend in terms of the Mg distribution [56], Fuji et al. [148] obtained an interlayer mainly consisting of $Al_{18}Mg_3Ti_2$ after PWHT of FW Al4.6%Mg and Ti. Sohn et al. [28] investigated TLPB of Al and Ti using an Al–10%Si–1%Mg filler and found Mg to reduce the Al surface oxides at 620 °C bonding temperature and therefore to improve the diffusion in the Al–Ti interface. The diffusion of Si into Al as well as its reaction with Ti was found to be much slower. It was concluded, that Al_2O_3 and Mg reacted exothermal within 1 min of holding time to form MgO (see Fig. 20) and remove the oxide layer completely. The improved diffusion is in accordance with findings by Wilden et al. [53,58], that the minimum diffusion temperature for AA5056 is approximately 40 K lower than for cp Al, see Fig. 21. Compared to Al1%Mn and cp Al, the interlayer growth rate in Al4.6%Mg was around 10 times faster and in the direction of Al [148].

In deformation-based joining of Al–Mg-alloys to Ti, high joint efficiencies up to 100 % are reached even with ultra-thin or without IMC [57], though the present bonding mechanisms are not yet fully understood. On the other hand, Korolev et al. [152] found an increasing Mg content from 2 to 6 wt% to decrease the mechanical strength in EW to Ti, which was attributed to micro-cracks in the Al close to the interface.

8.7. Zinc

Zinc addition to Al lowers the solidus temperature of the alloy. According to Kar et al. [153], Zn and Ti form various IMCs and therefore reduce the direct interaction of Al and Ti. Consequently, formation of $TiAl_3$ might be decreased by the formation of $TiZn_3$ [154]. Additionally, the combination of Ti and Zn acts as a grain refiner in the IMC and therefore enhances the interface homogeneity [153].

The combination of a decrease in the solidus temperature and the hindered interaction between Al and Ti impedes the joining of Al–Cu–Zn alloys and Ti significantly. Ugurlu and Cakan [155] achieved joint efficiencies of ~35 % in FSBW using low heat input to avoid local melting and void formation. Österreicher et al. [118] recently improved the joint efficiency for AA7075 to ~70 % by reducing the heat input compared to conventional FSBW due to no contact between shoulder and Ti but

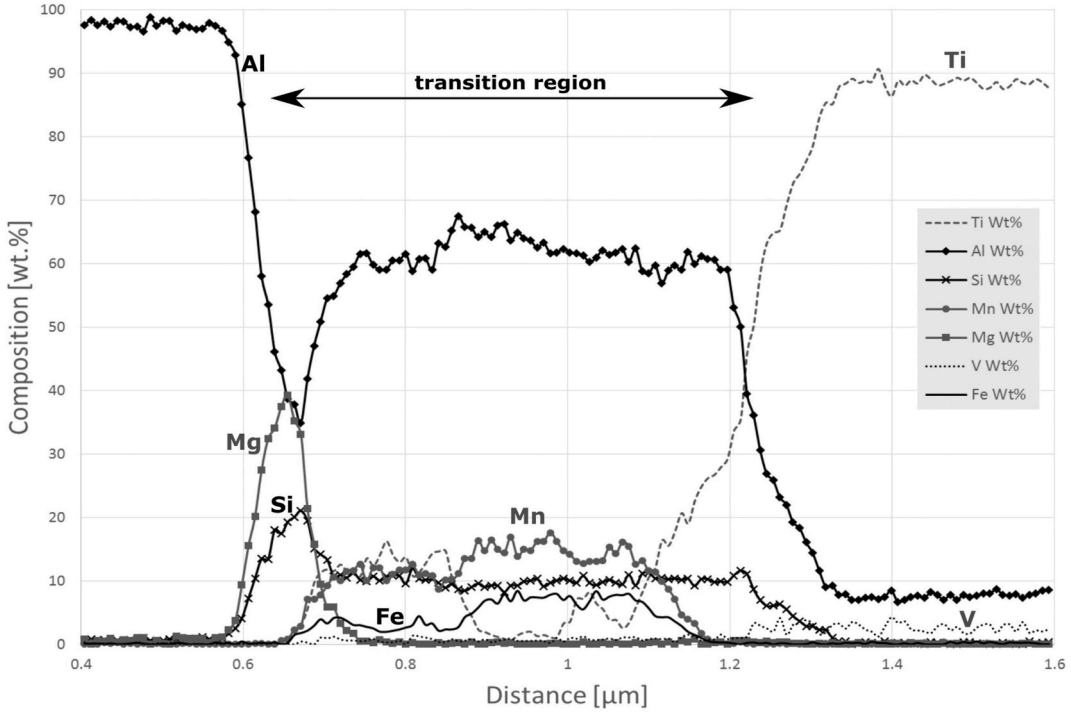

Fig. 19. EDS analysis of weld interface region of FW AA6082 and Ti6Al4V, linescan across weld interface, passing through transition region showing alternation in Mn and Ti content; compositions in wt%, reprinted from Ref. [149] with permission from Elsevier.

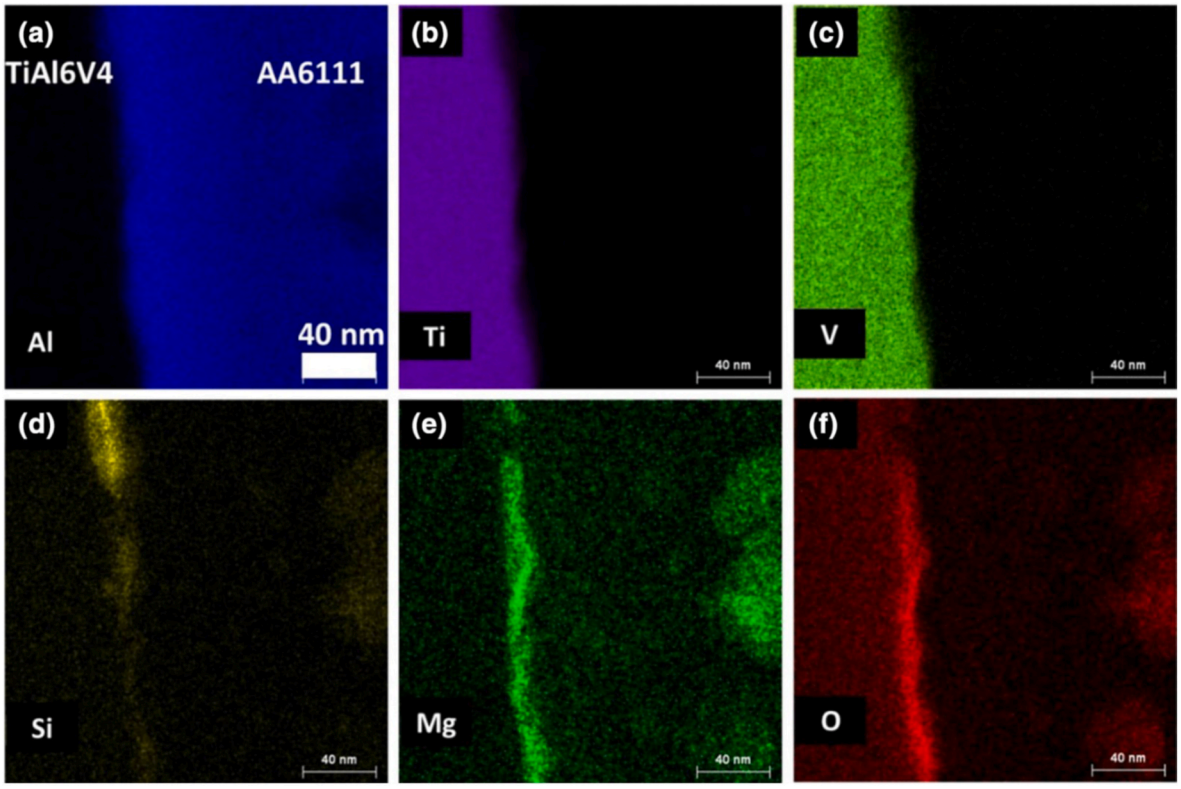

Fig. 20. STEM-EDS element maps in the AA6111/Ti6Al4V interface region after UW showing enrichment of Si (d), Mg (e) and O (f) in the interface, reprinted from Ref. [132].

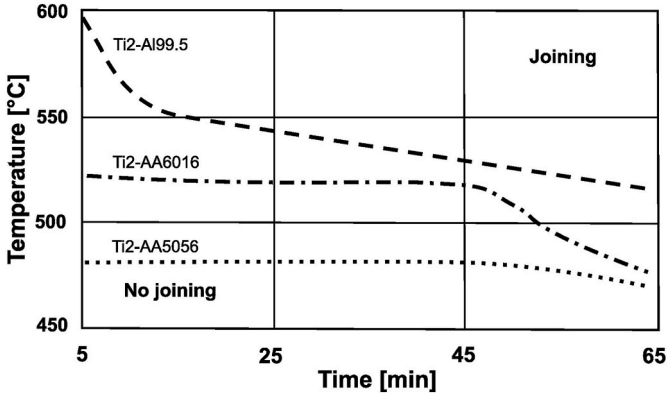

Fig. 21. Time-temperature-dependence of joint formation in DB of Ti Gr. 2 to cp Al, AA5056 and AA6016, combined from Refs. [53,58].

simultaneous plastic deformation of 0.3–0.4 mm of the Ti interface. Also here, no IMC in the interface was observed. Amirov et al. [156] used under-water FSLW ad low tool rotation rates to increase the joint strength in joining of AA7075 and Ti6Al4V. In EW, Xia et al. [157] successfully used a commercially pure Al interlayer to address the differing physical properties of Al–Cu–Zn alloy and Ti as well as to avoid cracking under plastic deformation due to limited ductility of high-strength Al–Cu–Zn alloys.

8.8. Zirconium

Karpets et al. [158] studied the influence of Zirconium addition on the properties of $TiAl_3$ by arc melting. They found the crystal structure to change from $D0_{22}$ to $D0_{23}$ by increasing Zr concentration. As $D0_{23}$-$TiAl_3$ behaves more ductile, Lv et al. [159] estimated Zr to improve the mechanical strength of Al–Ti-joints. Additionally, formation of (Ti,Zr) Al_3 is detected, which, according to Lv et al. [159], leads to a more heterogeneous nucleation and therefore fine-grained morphology of the IMC that would improve ductility. Though both investigations used arc-welding, the same effects can be assumed in SSSJ but have not yet been proven.

8.9. Summary

The previous mentioned observations are summarised in Table 3. From these observations, it can be concluded that alloying elements have a significant influence on the interface evolution in SSSJ of Al and Ti, though it is not yet systematically analysed. Effects can be expected through their influence on the base-material strength and thermo-mechanical properties, their diffusivity and chemical affinity as well as influence on ductility of IMC. Accumulation is seen in DB and PWHT, but variations in chemical affinities can also be expected in deformation-based processes. Regarding the influence on mechanical strength of the joint, Mg and Zr seem to have positive and Al, Cu, Si and Zn negative effects. Formation of IMC is promoted by Mg but retarded by V, Cu, Si and Zn.

9. Critical discussion and future research directions

As revealed above, great efforts have been made in recent years to analyse and optimise the process of joining Al to Ti alloys by SSSJ-techniques. However, the generalisability of the knowledge generated is doubtful, as important process parameters like the actual interface temperature cycle, the influence of the base metal's chemical composition or the mechanical impact have not been investigated systematically.

As described, plastic deformation enhances the diffusion between Al and Ti, however, there is no quantification of this effect which prevents comparison between various processes. Furthermore, even for thermally

Table 3
Overview on influence of alloying elements on the joint formation between Al and Ti.

Alloying Element	Intermetallic Compounds	Observations and Remarks
ALUMINIUM	$TiAl_3$, TiAl, Ti_3Al, $TiAl_2$, Ti_2Al_5	– Causes longer and faster linear growth of IMC [4] – Reduces concentration gradient [136]
VANADIUM		– Accumulates in $TiAl_3$, retards IMC formation in combination with Si and Mg [61]
COPPER	Al_2Cu, Al_aCu_b, Cu_cTi_d	– Retards IMC growth by increase of activation energy [138] – Accumulates in $TiAl_3$ and absorbs diffusing atoms [131] by formation of AlCu and AlTi-IMC [140] – Decreases solidus temperature of Al which promotes partial melting [125, 145]
MANGANESE		– Enriches in the interface [47] – Alternates with Ti [149]
SILICON	$Ti(Al,Si)_3$, Ti_5Si_3, $Ti_7Al_5Si_{12}$	– Concentrates in interface directly during joining [56], – Replaces Al in the IMC up to 15 % [150], – Hinders diffusion of Al to Ti [86] and increases diffusion temperature by 40 K [53]
MAGNESIUM	$Al_{18}Mg_3Ti_2$	– Reduces surface oxides on Al [28] and accelerates diffusion by factor 10 [148] – Diffuses into the IMC [61]
ZINC	$TiZn_3$ and other	– Hinders interaction between Al and Ti by formation of TiZn-IMC [153] – Decreases solidus temperature of Al which promotes partial melting
ZIRCONIUM	$(Ti,Zr)Al_3$	– Changes crystal structure of $TiAl_3$ to less brittle $D0_{23}$ [159]

induced diffusion, the diffusion coefficients of Al in Ti and vice versa are not reliably revealed, see Fig. 8, not to mention diffusion coefficients in three-phase systems or complex technological alloys. Systematic investigation and subsequent modelling of diffusion and chemical reaction between Al-alloys and Ti-alloys is therefore needed. This should include effects of temperature as well as plastic deformation before or during joining and clarify the differences in temperature and deformation-driven processes.

The plastic deformation of Ti and the exothermic formation of $TiAl_3$ lead to locally enhanced temperatures due to the low heat dissipation in Ti. This might even lead to an exceeding of the Al solidus temperatures. Interface temperature measurements in SSSJ of Al and Ti are rarely reported and often attempted by extrapolation towards the interface, which causes significant measurement uncertainties. Therefore, it must be doubted that solid-state joining is a correct process description in several cases, instead semi solid-state joining might be more appropriate. Direct measurement of the interface temperature within the process as well as incorporating also the heat generated by the reaction of Al and Ti (and alloying elements) within the interface in temperature field models is therefore recommended. Also, a detailed analysis of the interface regarding evidence for partial melting (e.g. solidification cracks, dendritic microstructure) is needed even if processes are generally known as solid-state.

Another aspect regarding assumptions and approximate comparisons involves PWHT approaches. Some key statements, such as the critical 5 μm thickness of IMC mentioned above, refer directly to subsequently generated IMCs. Here, properties such as grain size and orientation could be fundamentally different. Systematic investigations into the extent of differences between IMCs that are formed during joining and those that grow during PWHT are needed. This gets even more important when alloying elements are involved which have differing diffusion coefficient and reaction kinetics compared to the binary Al–Ti system. Optimum mechanical properties have to be considered as a complex interaction of phase composition, layer thickness, residual stresses and lattice defects.

For fusion welding as well as for DB of Al and Ti, the occurrence of IMC, especially $TiAl_3$, is an undoubted side-effect. As Al and Ti have a high chemical affinity towards each other, high process temperatures or long process times lead to growth of IMC layer(s). Furthermore, an increase in the thickness of a brittle IMC reasonably deteriorates the joint strength. This has been demonstrated by Kim and Fuji [15] by applying PWHT to FW couples of Al and Ti.

However, deformation-based approaches like FSW, RB or FW use (severe) plastic deformation instead to initialise the diffusion between Al and Ti which seems not to stimulate the growth of IMC. Additionally, the material flow especially in FSW leads to abrasion of the Ti surface and therefore dispersion of the Ti particles as well as growing IMC. Nevertheless, multiple researchers found IMC thicknesses to be in the sub-micrometre range. Additionally, in some cases, even no IMC was detectible while acceptable joint strength was achieved. It is questionable, whether diffusive bonding without simultaneous chemical reaction is possible or if the thickness of the IMC was below the resolution of the applied detection methods. Therefore, detailed investigations regarding the sequence of formation of diffusion layers and various IMCs of Al, Ti and alloying elements are needed to separate the diverse effects of strengthening and weakening the joint. Also, the detection and identification of IMC is performed in multiple ways. The first approach is the detection via back-scattered electrons in a scanning electron microscope (SEM). The different densities of Al, Ti and IMC enable the detection of different phases, however, it does not reveal the chemical composition, and the resolution is typically limited to approx. 1 μm. The second approach uses energy-dispersive X-ray spectroscopy (EDS) either in line-scanning or mapping of elemental distribution. Two aspects seem to be often not considered and lead to arguable results: First, the diameter of the electron beam and its spreading in the sample, which lower the resolution and blur the results in plane direction; second, the surface topography of the interface and the penetration depth of the beam might suggest a multi-elemental phase by just measuring an overlap. At least the second issue could be partially addressed by using transmission-EDS in thin lamellas. Furthermore, special attention should be given to the selection of investigated elements. In numerous cases, the main alloying elements are not included in the analysis so pure Al–Ti-IMC is stated. However, as shown in the previous section, alloying elements significantly influence the IMC formation. The most advanced approach to investigate the interface is X-ray diffraction (XRD), which serves information about the lattice constants within a defined volume and therefore the specific crystal structure. Though XRD and TEM investigation are technologically challenging, it is recommended for especially deformation-driven processes to analyse the interface in the nanometre scale. Here, nano-XRD of thin lamellae is believed to be a promising option.

10. Summary and conclusions

In the past 50 years, several approaches have been established to join Al and Ti alloys. One main challenge is to avoid an unnecessarily high amount of brittle intermetallic compound layers. For this reason, solid-state and semi-solid-state welding and weld-brazing techniques have been intensively applied. Several information on growth characteristics and effects of the IMCs are concluded from studies involving heat-treatments. Here, potential differences between heat-treated IMCs and as-welded IMCs need still to be clarified. Although there is no systematic investigation of fundamental factors in the various processes, based on the broad set of data available, some general statements can be given.

1. Significant interdiffusion of cp-Al and cp-Ti in annealed condition starts at temperatures above 520 °C. Up to the Al solidus

temperature, the influence of diffusion time is lower than that of the temperature.
2. Plastic deformation increases the diffusivity as well as reduces the diffusion start temperature by introducing lattice defects and removing oxide layers. Plastic deformation of the Ti alloy surface can also be induced by the Al material flow.
3. $TiAl_3$ is the only IMC formed directly in the diffusion process if TiAl and Ti_3Al are not forced by a low concentration of Al atoms at the specific point of formation in the matrix.
4. Plastic deformation reduces the transition point for the evolution of $TiAl_3$ IMC from 665 °C to ~550 °C and for the growth of IMC to even ~425 °C.
5. During deformation-based processes, besides $TiAl_3$, type–II–IMCs (especially Ti_2Al_5 and $TiAl_2$) can form.
6. The formation of a $TiAl_3$ layer has no significant barrier effect on the interdiffusion between Al and Ti.
7. Formation of a detectible IMC layer (>2 nm) is found not necessary for achieving high tensile properties.
8. The effect of IMCs on mechanical properties depends on their thickness and bonding to the base material. As diffusion is a precondition for IMC formation, their presence indicates the existence of proper diffusion bonding. Their growth deteriorates the mechanical properties due to their brittleness and the triaxial stresses caused by the significant difference in Young's modulus compared to the Al base material.
9. Despite the fact that plastic deformation allows for joining at lower temperatures, the process parameter window between incomplete bonding and partial melting of Al remains narrow for Al/Ti joints. This is further impaired by the fact that energy is normally introduced into the Al side so that Al has to bear the highest external impact.
10. Alloying elements influence the bonding between Al and Ti by deceleration (Cu; Si) or acceleration (Mg) of diffusion, formation of other IMCs (Cu; Si; Mg; Zn), change in lattice structure (Zr) and both the solidus temperature as well as viscoplastic properties (Cu; Zn).

Declaration of competing interest

The authors declare that they have no known competing financial interests or personal relationships that could have appeared to influence the work reported in this paper.

Acknowledgements

Funding by the Deutsche Forschungsgemeinschaft (DFG, German Research Foundation) – project number 464986536 - is gratefully acknowledged.

References

[1] Vaidya WV, Horstmann M, Ventzke V, Petrovski B, Koçak M, Kocik R, Tempus G. Improving interfacial properties of a laser beam welded dissimilar joint of aluminium AA6056 and titanium Ti6Al4V for aeronautical applications. J Mater Sci 2010;45:6242–54. https://doi.org/10.1007/s10853-010-4719-6.
[2] Rana H, Campanella D, Buffa G, Fratini L. Dissimilar titanium-aluminum skin-stringer joints by FSW: process mechanics and performance. Mater Manuf Process 2023;38:471–84. https://doi.org/10.1080/10426914.2022.2116044.
[3] Suslov AA. Brazing laminated structures of light alloys based on aluminium and titanium. Weld Int 1995;9:570–2. https://doi.org/10.1080/09507119509548853.
[4] van Loo F, Rieck G. Diffusion in the titanium-aluminium system—I. Interdiffusion between solid Al and Ti or Ti-Al alloys. Acta Metall 1973;21:61–71. https://doi.org/10.1016/0001-6160(73)90220-4.
[5] van Loo F, Rieck G. Diffusion in the titanium-aluminium system—Ii. Interdiffusion in the composition range between 25 and 100 at.% Ti. Acta Metall 1973;21:73–84. https://doi.org/10.1016/0001-6160(73)90221-6.
[6] Lin H-L, Chen P-A. Effects of parameters on welding performance of the Ti/Al butt-joint in advanced plasma-MIG hybrid welding. Int J Adv Manuf Technol 2024;130:2661–73. https://doi.org/10.1007/s00170-023-12849-1.
[7] Casalino G, Mortello M, Peyre P. Yb–YAG laser offset welding of AA5754 and T40 butt joint. J Mater Process Technol 2015;223:139–49. https://doi.org/10.1016/j.jmatprotec.2015.04.003.
[8] Chen S, Yang D, Li M, Zhang Y, Huang J, Yang J, Zhao X. Laser penetration welding of an overlap titanium-on-aluminum configuration. Int J Adv Manuf Technol 2016;87:3069–79. https://doi.org/10.1007/s00170-016-8732-z.
[9] Fernandes FAO, Gonçalves JJM, Pereira AB. Evaluation of laser lap weldability between the titanium alloy Ti-6Al-4V and aluminum alloy 6060-T6. Crystals 2023;13:1448. https://doi.org/10.3390/cryst13101448.
[10] Malikov A, Vitoshkin I, Orishich A, Filippov A, Karpov E. Microstructure and mechanical properties of laser welded joints of Al-Cu-Li and Ti-Al-V alloys. J Manuf Process 2020;53:201–12. https://doi.org/10.1016/j.jmapro.2020.02.010.
[11] Anchev A, Kaisheva D, Kotlarski G, Dunchev V, Stoyanov B, Ormanova M, Atanasova M, Todorov V, Daskalova P, Valkov S. Welding of Ti6Al4V and Al6082-T6 alloys by a scanning electron beam. Metals 2023;13:1252. https://doi.org/10.3390/met13071252.
[12] Havlík P, Kouřil J, Foret R, Dlouhy I, Enzinger N, Wiednig C. Evaluation of weldability of titanium alloy Ti-6Al-4V and aluminum alloy 6061 produced by electron beam welding. MS 2016;879:714–9. https://doi.org/10.4028/www.scientific.net/MSF.879.714.
[13] Gadakh VS, Badheka VJ, Mulay AS. Solid-state joining of aluminum to titanium: a review. Proc Inst Mech Eng Part L 2021;235:1757–99. https://doi.org/10.1177/14644207211010839.
[14] Da Silva EP, Castro CAC, Correa EO. Joining of Ti6Al4V/Al7075-T6 alloys without forming an intermediate layer by the GMAW process. Int J Adv Manuf Technol 2025;136:5083–102. https://doi.org/10.1007/s00170-025-15131-8.
[15] Kim Y-C, Fuji A. Factors dominating joint characteristics in Ti – al friction welds. Sci Technol Weld Join 2002;7:149–54. https://doi.org/10.1179/136217102225004185.
[16] Kar A, Suwas S, Kailas SV. Multi-length scale characterization of microstructure evolution and its consequence on mechanical properties in dissimilar friction stir welding of titanium to aluminum. Metall Mater Trans 2019;50:5153–73. https://doi.org/10.1007/s11661-019-05409-4.
[17] Wang T, Li X, Zhang Y, Li H, Zhang B, Feng J. Regulating the interfacial morphology of electron beam welded pure Ti/2024Al dissimilar joint. J Mater Process Technol 2017;245:227–31. https://doi.org/10.1016/j.jmatprotec.2017.02.028.
[18] Lv SX, Jing X, Huang Y, Xu YQ, Zheng CQ, Yang SQ. Investigation on TIG arc welding–brazing of Ti/Al dissimilar alloys with Al based fillers. Sci Technol Weld Join 2012;17:519–24. https://doi.org/10.1179/1362171812Y.0000000041.
[19] Cooke KO, Atieh AM. Current trends in dissimilar diffusion bonding of titanium alloys to stainless steels, aluminium and magnesium. JMMP 2020;4:39. https://doi.org/10.3390/jmmp4020039.
[20] Jain, S.; Bhuva, K.; Patel, P.; Badheka, V. J. A review on dissimilar friction stir welding of aluminum alloys to Titanium Alloys, 757, 415–425. DOI: 10.1007/978-981-13-1966-2_37.
[21] Khalafe WH, Sheng EL, Bin Isa MR, Omran AB, Shamsudin SB. The effect of friction stir welding parameters on the weldability of aluminum alloys with similar and dissimilar metals: review. Metals 2022;12:2099. https://doi.org/10.3390/met12122099.
[22] Yu M, Zhao H, Jiang Z, Zhang Z, Xu F, Zhou L, Song X. Influence of welding parameters on interface evolution and mechanical properties of FSW Al/Ti lap joints. J Mater Sci Technol 2019;35:1543–54. https://doi.org/10.1016/j.jmst.2019.04.002.
[23] Beygi R, Galvão I, Akhavan-Safar A, Pouraliakbar H, Fallah V, da Silva LFM. Effect of alloying elements on intermetallic formation during friction stir welding of dissimilar metals: a critical review on aluminum/steel. Metals 2023;13:768. https://doi.org/10.3390/met13040768.
[24] He P, Yue X, Zhang JH. Hot pressing diffusion bonding of a titanium alloy to a stainless steel with an aluminum alloy interlayer. Mater Sci Eng, A 2008;486:171–6. https://doi.org/10.1016/j.msea.2007.08.076.
[25] Klassen T, Oehring M, Bormann R. The early stages of phase formation during mechanical alloying of Ti–Al. J Mater Res 1994;9:47–52. https://doi.org/10.1557/JMR.1994.0047.
[26] Sujata M, Bhargava S, Sangal S. On the formation of TiAl3 during reaction between solid Ti and liquid Al. J Mater Sci Lett 1997;16:1175–8. https://doi.org/10.1007/BF02765402.
[27] Kazakov NF. Apparatus for diffusion joining in a vacuum of metals, alloys and materials different in kind. Oct 5, 1964. US19640401289 19641005.
[28] Sohn WH, , Bong, H. H., Hong SH. Microstructure and bonding mechanism of Al/Ti bonded joint using Al–10Si–1Mg filler metal. Mater Sci Eng, A 2003;355:231–40. https://doi.org/10.1016/S0921-5093(03)00070-4.
[29] Kazakov NF. Diffusion bonding of materials. Oxford: Pergamon Pr; 1981.
[30] MacDonald WD, Eagar TW. Transient liquid phase bonding. Annu Rev Mater Sci 1992;22:23–46. https://doi.org/10.1146/annurev.ms.22.080192.000323.
[31] Tsuji N, Saito Y, Utsunomiya H, Tanigawa S. Ultra-fine grained bulk steel produced by accumulative roll-bonding (ARB) process. Scr Mater 1999;40:795–800. https://doi.org/10.1016/S1359-6462(99)00015-9.
[32] Crossland B, Williams JD, Shribman V. Developments in explosive welding. Aircraft Eng Aero Technol 1968;40:11–3. https://doi.org/10.1108/eb034451.
[33] Crossland B. Friction welding. Contemp Phys 1971;12:559–74. https://doi.org/10.1080/00107517108205660.
[34] Harthoorn JL. Ultrasonic metal welding. 1978.
[35] Thomas WM, Nicholas ED, Needham JC, Murch MG, Temple SP, Dawes CJ. Friction welding. Aug 1, 1994. US19940244612 19940801.

[36] Mishra RS, Ma ZY. Friction stir welding and processing. Mater Sci Eng R Rep 2005;50:1–78. https://doi.org/10.1016/j.mser.2005.07.001.
[37] Schilling C, Dos SJ. Device for joining by friction stir welding at least two workpieces that adjoin at least in the contact zone. Nov 17, 2000. WO2000DE04055 20001117.
[38] Suhuddin U, Fischer V, dos Santos JF. The thermal cycle during the dissimilar friction spot welding of aluminum and magnesium alloy. Scr Mater 2013;68:87–90. https://doi.org/10.1016/j.scriptamat.2012.09.008.
[39] Jacques P, Van DRC, Simar A. Method for welding at least two layers. Apr 29, 2013. WO2013EP58844 20130429.
[40] van der Rest C, Jacques PJ, Simar A. On the joining of steel and aluminium by means of a new friction melt bonding process. Scr Mater 2014;77:25–8. https://doi.org/10.1016/j.scriptamat.2014.01.008.
[41] Ma M, Huo P, Liu WC, Wang GJ, Wang DM. Microstructure and mechanical properties of Al/Ti/Al laminated composites prepared by roll bonding. Mater Sci Eng, A 2015;636:301–10. https://doi.org/10.1016/j.msea.2015.03.086.
[42] Dressler U, Biallas G, Alfaro Mercado U. Friction stir welding of titanium alloy TiAl6V4 to aluminium alloy AA2024-T3. Mater Sci Eng, A 2009;526:113–7. https://doi.org/10.1016/j.msea.2009.07.006.
[43] Choi J-W, Liu H, Fujii H. Dissimilar friction stir welding of pure Ti and pure Al. Mater Sci Eng, A 2018;730:168–76. https://doi.org/10.1016/j.msea.2018.05.117.
[44] Foadian F, Soltanieh M, Adeli M, Etminanbakhsh M. A study on the formation of intermetallics during the heat treatment of explosively welded Al-Ti multilayers. Metall Mater Trans A 2014;45:1823–32. https://doi.org/10.1007/s11661-013-2144-6.
[45] Li B, Shen Y, Luo L, Hu W. Effects of processing variables and heat treatments on Al/Ti-6Al-4V interface microstructure of bimetal clad-plate fabricated via a novel route employing friction stir lap welding. J Alloys Compd 2016;658:904–13. https://doi.org/10.1016/j.jallcom.2015.10.288.
[46] Geyer M, Avettand-Fènoël M-N, Vidal V, Rezaï-Aria F, Boher C. Multi-scale effects of the tool shape and length on the interfacial microstructure and the mechanical behaviour of Al2024/Ti-6Al-4V lap friction stir welds. J Manuf Process 2024;113:360–72. https://doi.org/10.1016/j.jmapro.2024.01.056.
[47] Kalinenko A, Dolzhenko P, Borisova Y, Malopheyev S, Mironov S, Kaibyshev R. Tailoring of dissimilar friction stir lap welding of aluminum and titanium. Materials 2022;15. https://doi.org/10.3390/ma15238418.
[48] Ji SM, Jang SM, Lee YS, Kwak HM, Choi JM, Joun MS. Characterization of Ti-6Al-4V alloy in the temperature range of warm metal forming and fracture analysis of the warm capping process. J Mater Res Technol 2022;18:1590–606. https://doi.org/10.1016/j.jmrt.2022.03.066.
[49] Wu LH, Xue P, Xiao BL, Ma ZY. Achieving superior low-temperature superplasticity for lamellar microstructure in nugget of a friction stir welded Ti-6Al-4V joint. Scr Mater 2016;122:26–30. https://doi.org/10.1016/j.scriptamat.2016.05.020.
[50] Kalinenko A, Dolzhenko P, Malopheyev S, Yuzbekova D, Borisova Y, Shishov I, Mishin V, Mironov S, Kaibyshev R. Interfacial microstructure produced during dissimilar AA6013/Ti-6Al-4V friction stir lap welding under zero-penetration condition. Metals 2023;13:1667. https://doi.org/10.3390/met13101667.
[51] Ramana CV, Choi BS, Smith RJ, Hutchinson R, Stuk SP, Park BS, Saleh AA, Jeon DR. Thermal stability of thin Ti films on Al single crystal surfaces. J Vac Sci Technol A: Vacuum, Surfaces, and Films 2003;21:1326–31. https://doi.org/10.1116/1.1564039.
[52] Gachon J-C, Rogachev AS, Grigoryan HE, Illarionova EV, Kuntz J-J, Kovalev D, Nosyrev AN, Sachkova NV, Tsygankov PA. On the mechanism of heterogeneous reaction and phase formation in Ti/Al multilayer nanofilms. Acta Mater 2005;53:1225–31. https://doi.org/10.1016/j.actamat.2004.11.016.
[53] Wilden J, Bergmann JP. Manufacturing of titanium/aluminium and titanium/steel joints by means of diffusion welding. Weld Cut 2004;56:285–90.
[54] Thiyaneshwaran N, Sivaprasad K, Ravisankar B. Nucleation and growth of TiAl3 intermetallic phase in diffusion bonded Ti/Al metal intermetallic laminate. Sci Rep 2018;8:16797. https://doi.org/10.1038/s41598-018-35247-0.
[55] Wei Y, Aiping W, Guisheng Z, Jialie R. Formation process of the bonding joint in Ti/Al diffusion bonding. Mater Sci Eng, A 2008;480:456–63. https://doi.org/10.1016/j.msea.2007.07.027.
[56] Bang K-S, Lee K-J, Bang H-S, Bang H-S. Interfacial microstructure and mechanical properties of dissimilar friction stir welds between 6061-T6 aluminum and Ti-6% Al-4%V alloys. Mater Trans 2011;52:974–8. https://doi.org/10.2320/matertrans.L-MZ201114.
[57] Fuji A, Kimura M, North TH, Ameyama K, Aki M. Mechanical properties of titanium-5083 aluminium alloy friction joints. Mater Sci Technol 1997;13:673–8. https://doi.org/10.1179/mst.1997.13.8.673.
[58] Wilden J, Bergmann JP, Jahn S. Mechanical properties and processing of low-temperature diffusion-welded hybrid joints. Adv Eng Mater 2006;8:212–8. https://doi.org/10.1002/adem.200600006.
[59] Rajakumar S, Balasubramanian V. Diffusion bonding of titanium and AA 7075 aluminum alloy dissimilar joints—process modeling and optimization using desirability approach. Int J Adv Manuf Technol 2016;86:1095–112. https://doi.org/10.1007/s00170-015-8223-7.
[60] Xu L, Cui YY, Hao YL, Yang R. Growth of intermetallic layer in multi-laminated Ti/Al diffusion couples. Mater Sci Eng, A 2006;435–436:638–47. https://doi.org/10.1016/j.msea.2006.07.077.
[61] Liu M, Zhang C, Meng Z, Zhao G, Chen L. TiAl3 nucleation mechanism and atomic-scale interface features in the Al/Ti composite structures. Compos B Eng 2021;226:109331. https://doi.org/10.1016/j.compositesb.2021.109331.
[62] Assari AH, Eghbali B. Solid state diffusion bonding characteristics at the interfaces of Ti and Al layers. J Alloys Compd 2019;773:50–8. https://doi.org/10.1016/j.jallcom.2018.09.253.
[63] Yu H, Lu C, Tieu AK, Li H, Godbole A, Kong C. Annealing effect on microstructure and mechanical properties of Al/Ti/Al laminate sheets. Mater Sci Eng, A 2016;660:195–204. https://doi.org/10.1016/j.msea.2016.02.087.
[64] Cui X, Fan G, Geng L, Wang Y, Huang L, Peng H-X. Growth kinetics of TiAl3 layer in multi-laminated Ti–(TiB2/Al) composite sheets during annealing treatment. Mater Sci Eng, A 2012;539:337–43. https://doi.org/10.1016/j.msea.2012.01.107.
[65] Luo J-G, Acoff VL. Using cold roll bonding and annealing to process Ti/Al multi-layered composites from elemental foils. Mater Sci Eng, A 2004;379:164–72. https://doi.org/10.1016/j.msea.2004.01.021.
[66] Bergner D. Diffusion von Fremdelementen in Aluminium. Neue Hutte 1984;29:207–10.
[67] Köppers M, Herzig C, Friesel M, Mishin Y. Intrinsic self-diffusion and substitutional Al diffusion in α-Ti. Acta Mater 1997;45:4181–91. https://doi.org/10.1016/S1359-6454(97)00078-5.
[68] Räisänen J, Anttila A, Keinonen J. Diffusion of aluminum in ion-implanted α-Ti. J Appl Phys 1985;57:613–4. https://doi.org/10.1063/1.334747.
[69] Solid metals and alloys. DDF 1971;5:271–313. https://doi.org/10.4028/www.scientific.net/DDF.5.271.
[70] AlHazaa A, Khan TI. Diffusion bonding of Al7075 to Ti–6Al–4V using Cu coatings and Sn–3.6Ag–1Cu interlayers. J Alloys Compd 2010;494:351–8. https://doi.org/10.1016/j.jallcom.2010.01.037.
[71] Liquid Metals and Alloys. DDF 1971;5:614–25. https://doi.org/10.4028/www.scientific.net/DDF.5.614.
[72] Robson JD. Deformation enhanced diffusion in aluminium alloys. Metall Mater Trans A 2020;51:5401–13. https://doi.org/10.1007/s11661-020-05960-5.
[73] Nan X, Zhao H, Ma C, Sun S, Sun G, Xu Z, Zhou L, Wang R, Song X. Interface characterization and formation mechanism of Al/Ti dissimilar joints of refill friction stir spot welding. Int J Adv Manuf Technol 2023;126:1539–51. https://doi.org/10.1007/s00170-023-11226-2.
[74] Zhao H, Yu M, Jiang Z, Zhou L, Song X. Interfacial microstructure and mechanical properties of Al/Ti dissimilar joints fabricated via friction stir welding. J Alloys Compd 2019;789:139–49. https://doi.org/10.1016/j.jallcom.2019.03.043.
[75] Wang P, Chen Z, Hu C, Li B, Lin J, Liu Q. Effects of annealing on the interface microstructures and mechanical properties of hot roll bonded Ti6Al4V/AA6061 clad sheets. J Mater Res Technol 2020;9:11813–25. https://doi.org/10.1016/j.jmrt.2020.08.070.
[76] Ma Z, Sun X, Ji S, Wang Y, Yue Y. Influences of ultrasonic on friction stir welding of Al/Ti dissimilar alloys under different welding conditions. Int J Adv Manuf Technol 2021;112:2573–82. https://doi.org/10.1007/s00170-020-06481-6.
[77] Li H, Zhang H, Liu X, Sun R, Gao Q, Ma K, Song J, Zhao Y. Weak penetration strategy combined with post-weld aging treatment to optimize interface joining for dissimilar friction stir lap welded aluminum and titanium alloys. Mater Char 2025;224:115097. https://doi.org/10.1016/j.matchar.2025.115097.
[78] Chen YC, Nakata K. Microstructural characterization and mechanical properties in friction stir welding of aluminum and titanium dissimilar alloys. Mater Des 2009;30:469–74. https://doi.org/10.1016/j.matdes.2008.06.008.
[79] Huang Y, Lv Z, Wan L, Shen J, dos Santos JF. A new method of hybrid friction stir welding assisted by friction surfacing for joining dissimilar Ti/Al alloy. Mater Lett 2017;207:172–5. https://doi.org/10.1016/j.matlet.2017.07.081.
[80] Raman A, Schubert K. Über den Aufbau einiger zu TiAl 3 verwandter Legierungsreihen. Int J Mater Res 1965;56:44–52. https://doi.org/10.1515/ijmr-1965-560109.
[81] Zhang Q, Xiao BL, Ma ZY. Mechanically activated effect of friction stir processing in Al–Ti reaction. Mater Chem Phys 2013;139:596–602. https://doi.org/10.1016/j.matchemphys.2013.01.062.
[82] Eremenko VN, Natanzon YV, Petrishchev VY. Kinetics of formation of the TiAl3 phase in the Ti-Al system. Powder Metall Met Ceram 1987;26:118–22. https://doi.org/10.1007/BF00794126.
[83] Levitas VI, Nesterenko VF, Meyers MA. Strain-induced structural changes and chemical reactions—I. Thermomechanical and kinetic models. Acta Mater 1998;46:5929–45. https://doi.org/10.1016/S1359-6454(98)00215-8.
[84] Levitas VI, Nesterenko VF, Meyers MA. Strain-induced structural changes and chemical reactions—Ii. Modelling of reactions in shear band. Acta Mater 1998;46:5947–63. https://doi.org/10.1016/S1359-6454(98)00214-6.
[85] Fronczek DM, Wojewoda-Budka J, Chulist R, Sypien A, Korneva A, Szulc Z, Schell N, Zieba P. Structural properties of Ti/Al clads manufactured by explosive welding and annealing. Mater Des 2016;91:80–9. https://doi.org/10.1016/j.matdes.2015.11.087.
[86] Fuji A. In situ observation of interlayer growth during heat treatment of friction weld joint between pure titanium and pure aluminium. Sci Technol Weld Join 2002;7:413–6. https://doi.org/10.1179/136217102225006903.
[87] Plaine AH, Suhuddin U, Afonso C, Alcântara NG, dos Santos JF. Interface formation and properties of friction spot welded joints of AA5754 and Ti6Al4V alloys. Mater Des 2016;93:224–31. https://doi.org/10.1016/j.matdes.2015.12.170.
[88] Kar A, Kailas SV, Suwas S. Formation sequence of intermetallics and kinetics of reaction layer growth during solid state reaction between titanium and aluminum. Materialia 2020;11:100702. https://doi.org/10.1016/j.mtla.2020.100702.
[89] Shouzheng W, Yajiang L, Juan W, Kun L, Pengfei Z. Microstructure and joining mechanism of Ti/Al dissimilar joint by pulsed gas metal arc welding. Int J Adv Manuf Technol 2014;70:1137–42. https://doi.org/10.1007/s00170-013-5290-5.

[90] Tanaka T, Nezu M, Uchida S, Hirata T. Mechanism of intermetallic compound formation during the dissimilar friction stir welding of aluminum and steel. J Mater Sci 2020;55:3064–72. https://doi.org/10.1007/s10853-019-04106-2.
[91] Leo P, D'Ostuni S, Casalino G. Low temperature heat treatments of AA5754-Ti6Al4V dissimilar laser welds: microstructure evolution and mechanical properties. Opt Laser Technol 2018;100:109–18. https://doi.org/10.1016/j.optlastec.2017.09.039.
[92] Moradi MJ, Enayati MH, Karimzadeh F, Izadi M. Production of Al-Ti composite by a combination of accumulative roll bonding and friction stir processing. J Mater Eng Perform 2023;103:12. https://doi.org/10.1007/s11665-023-07995-2.
[93] Gao M, Chen C, Gu Y, Zeng X. Microstructure and tensile behavior of laser arc hybrid welded dissimilar Al and Ti alloys. Materials 2014;7:1590–602. https://doi.org/10.3390/ma7031590.
[94] Zhang Z, Huang J, Fu J, Nie P, Zhang S. Microstructure and mechanical properties of laser welded-brazed titanium/aluminum joints assisted by titanium mesh interlayer. J Mater Process Technol 2022;302:117502. https://doi.org/10.1016/j.jmatprotec.2022.117502.
[95] Sundar AS, Mugada KK, Kumar A. Enhancing microstructural, textural, and mechanical properties of Al–Ti dissimilar joints via static shoulder friction stir welding. J Manuf Sci Eng 2024;146:6242. https://doi.org/10.1115/1.4063358.
[96] Plaine AH, Suhuddin U, Alcântara NG, dos Santos JF. Fatigue behavior of friction spot welds in lap shear specimens of AA5754 and Ti6Al4V alloys. Int J Fatig 2016;91:149–57. https://doi.org/10.1016/j.ijfatigue.2016.06.005.
[97] Yazdanian S, Ales S, Chen ZW. Effects of pin size and of using an interlayer on interface bonding and fatigue strength of AA2024 to Ti6Al4V lap joints made using friction stir welding. Weld World 2024;68:2217–33. https://doi.org/10.1007/s40194-024-01798-2.
[98] Wei Y, Li J, Xiong J, Huang F, Zhang F, Raza SH. Joining aluminum to titanium alloy by friction stir lap welding with cutting pin. Mater Char 2012;71:1–5. https://doi.org/10.1016/j.matchar.2012.05.013.
[99] Kimura M, Nakamura S, Kusaka M, Seo K, Fuji A. Mechanical properties of friction welded joint between Ti–6Al–4V alloy and Al–Mg alloy (AA5052). Sci Technol Weld Join 2005;10:666–72. https://doi.org/10.1179/174329305X57455.
[100] Rostami H, Nourouzi S, Jamshidi Aval H. Analysis of welding parameters effects on microstructural and mechanical properties of Ti6Al4V and AA5052 dissimilar joint. J Mech Sci Technol 2018;32:3371–7. https://doi.org/10.1007/s12206-018-0640-8.
[101] Ma Z, Jin Y, Ji S, Meng X, Ma L, Li Q. A general strategy for the reliable joining of Al/Ti dissimilar alloys via ultrasonic assisted friction stir welding. J Mater Sci Technol 2019;35:94–9. https://doi.org/10.1016/j.jmst.2018.09.022.
[102] Bang H-S, Bang H, Song H, Joo S. Joint properties of dissimilar Al6061-T6 aluminum alloy/Ti–6%Al–4%V titanium alloy by gas tungsten arc welding assisted hybrid friction stir welding. Mater Des 2013;51:544–51. https://doi.org/10.1016/j.matdes.2013.04.057.
[103] Plaine AH, Gonzalez AR, Suhuddin UFH, dos Santos JF, Alcântara NG. Process parameter optimization in friction spot welding of AA5754 and Ti6Al4V dissimilar joints using response surface methodology. Int J Adv Manuf Technol 2016;85:1575–83. https://doi.org/10.1007/s00170-015-8055-5.
[104] Plaine AH, Gonzalez AR, Suhuddin U, dos Santos JF, Alcântara NG. The optimization of friction spot welding process parameters in AA6181-T4 and Ti6Al4V dissimilar joints. Mater Des 2015;83:36–41. https://doi.org/10.1016/j.matdes.2015.05.082.
[105] Chen Y, Li Y, Shi L, Wu C, Li S, Gao S. Optimizing the shoulder diameter for double side friction stir welding of medium-thick TC4/AA2024 dissimilar alloys by Taguchi optimization technique. Weld World 2023;67:1887–99. https://doi.org/10.1007/s40194-023-01537-z.
[106] Zhang X, Zhao F, Li L, Shi L, Wu C, Kumar A, Mironov S. Ultrasonic vibration enhanced friction stir welding of titanium to aluminum. Int J Mech Sci 2025;291–292:110191. https://doi.org/10.1016/j.ijmecsci.2025.110191.
[107] Beygi R, Zarezadeh Mehrizi M, Akhavan-Safar A, Safaei S, Loureiro A, Da Silva LFM. Design of friction stir welding for butt joining of aluminum to steel of dissimilar thickness: heat treatment and fracture behavior. Int J Adv Manuf Technol 2021;112:1951–64. https://doi.org/10.1007/s00170-020-06406-3.
[108] Lee KS, Bae SJ, Lee HW, Kang SH. Interface-correlated bonding properties for a roll-bonded Ti/Al 2-ply sheet. Mater Char 2017;134:163–71. https://doi.org/10.1016/j.matchar.2017.10.009.
[109] Li B, Zhang Z, Shen Y, Hu W, Luo L. Dissimilar friction stir welding of Ti–6Al–4V alloy and aluminum alloy employing a modified butt joint configuration: influences of process variables on the weld interfaces and tensile properties. Mater Des 2014;53:838–48. https://doi.org/10.1016/j.matdes.2013.07.019.
[110] Esmaeili A, Sbarufatti C, Hamouda AMS. Characteristics of Intermetallic compounds in dissimilar friction stir welding: a review. Metallogr Microstruct Anal 2019;8:445–61. https://doi.org/10.1007/s13632-019-00557-w.
[111] Sundar AS, Kumar A, Mugada KK. Explication of microstructural evolution and mode of recrystallization in dissimilar Al6061–Ti6Al4V friction stir welds. Trans Indian Inst Met 2023;76:2085–90. https://doi.org/10.1007/s12666-023-02910-8.
[112] Kar A. Mechanism of microstructure evolution and improved mechanical properties in two-pass friction stir welding of titanium to aluminum. Archiv Civ Mech Eng 2023;23:955. https://doi.org/10.1007/s43452-023-00770-z.
[113] Chen ZW, Yazdanian S. Microstructures in interface region and mechanical behaviours of friction stir lap Al6060 to Ti–6Al–4V welds. Mater Sci Eng, A 2015;634:37–45. https://doi.org/10.1016/j.msea.2015.03.017.
[114] Patel P, Rana H, Badheka VJ, Patel V, Li W. Effect of active heating and cooling on microstructure and mechanical properties of friction stir–welded dissimilar aluminium alloy and titanium butt joints. Weld World 2020;64:365–78. https://doi.org/10.1007/s40194-019-00838-6.
[115] Wu A, Song Z, Nakata K, Liao J, Zhou L. Interface and properties of the friction stir welded joints of titanium alloy Ti6Al4V with aluminum alloy 6061. Mater Des 2015;71:85–92. https://doi.org/10.1016/j.matdes.2014.12.015.
[116] Song Z, Nakata K, Wu A, Liao J, Zhou L. Influence of probe offset distance on interfacial microstructure and mechanical properties of friction stir butt welded joint of Ti6Al4V and A6061 dissimilar alloys. Mater Des 2014;57:269–78. https://doi.org/10.1016/j.matdes.2013.12.040.
[117] Grassel F, Klusemann B. Friction stir lap weld-brazing of AA7050 aluminium alloy to Ti6Al4V titanium alloy – limitations in dissimilar metal joining. Manuf Lett 2025;44:37–41. https://doi.org/10.1016/j.mfglet.2025.03.005.
[118] Österreicher JA, Pfeiffer C, Kunschert G, Weinberger T, Schlögl CM, Suppan W, Radlmayr KM. Dissimilar friction stir welding and post-weld heat treatment of Ti-6Al-4V and AA7075 producing joints of unprecedented strength. J Adv Join Process 2024;9:100213. https://doi.org/10.1016/j.jajp.2024.100213.
[119] Buffa G, Lisi M de, Sciortino E, Fratini L. Dissimilar titanium/aluminum friction stir welding lap joints by experiments and numerical simulation. Adv Manuf 2016;4:287–95. https://doi.org/10.1007/s40436-016-0157-2.
[120] Eliseev AA, Ermakova SA, Kolubaev EA. Effect of ultrasonic impact on the macrostructure and strength of dissimilar aluminum and titanium alloys joints produced by friction stir welding. Russ Phys J 2023;65:2210–5. https://doi.org/10.1007/s11182-023-02892-6.
[121] Plaine AH, Suhuddin UFH, Alcântara NG, dos Santos JF. Microstructure and mechanical behavior of friction spot welded AA6181-T4/Ti6Al4V dissimilar joints. Int J Adv Manuf Technol 2017;92:3703–14. https://doi.org/10.1007/s00170-017-0439-2.
[122] Krutzlinger M, Marstatt R, Suenger S, Luderschmid J, Zaeh MF, Haider F. Formation of joining mechanisms in friction stir welded dissimilar Al-Ti lap joints. AMR (Adv Magn Reson) 2014;966–967:510–20. https://doi.org/10.4028/www.scientific.net/AMR.966-967.510.
[123] Sundar AS, Mugada KK, Kumar A. Microstructural evolution, intermetallic formation, and mechanical performance of dissimilar Al6061–Ti6Al4V static shoulder friction stir welds. Adv Eng Mater 2023;25. https://doi.org/10.1002/adem.202300973.
[124] Liang G, Huang J, Zhou D, Li X, Li K, Zhu G, Liu Z, Chen X, Hu J. Study on explosive welding of A7075/A1060/Ti-6Al-4V and its mechanical properties. J Occup Med 2025;77:1844–58. https://doi.org/10.1007/s11837-024-06950-3.
[125] Kar A, Suwas S, Kailas SV. Two-pass friction stir welding of aluminum alloy to titanium alloy: a simultaneous improvement in mechanical properties. Mater Sci Eng, A 2018;733:199–210. https://doi.org/10.1016/j.msea.2018.07.057.
[126] Zhang X, Shi L, Luo H, Wu C, Mironov S. Numerical simulation of heat and mass transfer in novel stepped structure friction stir welding of Ti/Al dissimilar alloys. Int J Heat Mass Tran 2025;242:126803. https://doi.org/10.1016/j.ijheatmasstransfer.2025.126803.
[127] Kar A, Singh K, Kumar L. Effect of tool rotational speed and mechanisms associated with microstructure evolution and intermetallics formation in friction stir welding of aluminum alloy to titanium alloy. J Mater Eng Perform 2023;56:108. https://doi.org/10.1007/s11665-023-08407-1.
[128] Watanabe M, Feng K, Nakamura Y, Kumai S. Growth manner of intermetallic compound layer produced at welding interface of friction stir spot welded aluminum/steel lap joint. Mater Trans 2011;52:953–9. https://doi.org/10.2320/matertrans.L-MZ201120.
[129] Sundar AS, Kumar A, Mugada KK. Minimizing material flow in the dissimilar joining of Al6061 and Ti6Al4V to mitigate the adverse effects of intermetallic compounds. Mater Lett 2023;350:134956. https://doi.org/10.1016/j.matlet.2023.134956.
[130] Zhang Y, Su Z, Zhang D, Zhu Z. Microstructural and mechanical property analyses of Ti/Al/Ti laminated composites prepared by ultrasonic welding. Mater Res 2024;27. https://doi.org/10.1590/1980-5373-mr-2023-0538.
[131] Malikov A, Vitoshkin I, Orishich A, Filippov A, Karpov E. Effect of the aluminum alloy composition (Al-Cu-Li or Al-Mg-Li) on structure and mechanical properties of dissimilar laser welds with the Ti-Al-V alloy. Opt Laser Technol 2020;126:106135. https://doi.org/10.1016/j.optlastec.2020.106135.
[132] Zhang C, Robson JD, Haigh SJ, Prangnell PB. Interfacial segregation of alloying elements during dissimilar ultrasonic welding of AA6111 aluminum and Ti6Al4V titanium. Metall Mater Trans A 2019;50:5143–52. https://doi.org/10.1007/s11661-019-05395-7.
[133] Takemoto T, Okamoto I. Intermetallic compounds formed during brazing of titanium with aluminium filler metals. J Mater Sci 1988;23:1301–8. https://doi.org/10.1007/BF01154593.
[134] Brown AM, Ashby MF. Correlations for diffusion constants. Acta Metall 1980;28:1085–101. https://doi.org/10.1016/0001-6160(80)90092-9.
[135] Wilden J, Bergmann JP, Herz S. Properties of diffusion welded hybrid joints titanium/aluminum. Proceedings of the 3rd international brazing and soldering conference. 2006. p. 338–43.
[136] Aonuma M, Nakata K. Dissimilar metal joining of 2024 and 7075 aluminium alloys to titanium alloys by friction stir welding. Mater Trans 2011;52:948–52. https://doi.org/10.2320/matertrans.L-MZ201102.
[137] Yousaf M, Iqbal J, Ajmal M. Variables affecting growth and morphology of the intermetallic layer (Fe2Al5). Mater Char 2011;62:517–25. https://doi.org/10.1016/j.matchar.2011.03.004.
[138] Tardy J, Tu KN. Solute effect of Cu on interdiffusion in Al3Ti compound films. Phys Rev B 1985;32:2070–81. https://doi.org/10.1103/PhysRevB.32.2070.

[139] Mustafa SE, Rai RN, Firoz R. Enhancement of joint properties and reduction of intermetallics in FSW of highly dissimilar Al/Ti alloys. Weld World 2023;41:4563. https://doi.org/10.1007/s40194-023-01493-8.
[140] Kar A, Suwas S, Kailas SV. Significance of tool offset and copper interlayer during friction stir welding of aluminum to titanium. Int J Adv Manuf Technol 2019;100:435–43. https://doi.org/10.1007/s00170-018-2682-6.
[141] Xue P, Xiao BL, Ni DR, Ma ZY. Enhanced mechanical properties of friction stir welded dissimilar Al–Cu joint by intermetallic compounds. Mater Sci Eng, A 2010;527:5723–7. https://doi.org/10.1016/j.msea.2010.05.061.
[142] Kim S-Y, Jung S-B, Shur C-C, Yeon Y-M, Kim D-U. Mechanical properties of copper to titanium joined by friction welding. J Mater Sci 2003;38:1281–7. https://doi.org/10.1023/A:1022890611264.
[143] Ivanov A, Chumaevskii A, Amirov A, Utyaganova V, Savchenko N, Rubtsov V, Tarasov S. Features of structure and properties of lap-welded joints of aluminum alloy Al–4Cu–1Mg with titanium alloy Ti–6Al–4V, obtained by friction stir welding. Metals 2023;13:1385. https://doi.org/10.3390/met13081385.
[144] Amirov AI, Chumaevskii AV, Utyaganova VR, Gusarova AV, Gurianov DA, Rubtsov VE, Beloborodov VA, Sokolov PS, Kolubaev EA. Structure and properties of dissimilar joint of Ti and Al alloys obtained by friction stir welding. Russ Phys J 2023;66:970–7. https://doi.org/10.1007/s11182-023-03031-x.
[145] Zhang X, Shi L, Wu C, Yang C, Gao S. Multi-phase modelling of heat and mass transfer during Ti/Al dissimilar friction stir welding process. J Manuf Process 2023;94:240–54. https://doi.org/10.1016/j.jmapro.2023.03.037.
[146] Zhang CQ, Robson JD, Prangnell PB. Dissimilar ultrasonic spot welding of aerospace aluminum alloy AA2139 to titanium alloy TiAl6V4. J Mater Process Technol 2016;231:382–8. https://doi.org/10.1016/j.jmatprotec.2016.01.008.
[147] Li Y, Shi L, Wu CS, Jiang Y. Achieving high property medium-thick Ti/Al dissimilar joints by double side friction stir welding. Sci Technol Weld Join 2022;27:655–63. https://doi.org/10.1080/13621718.2022.2106019.
[148] Fuji A, Ikeuchi K, Sato YS, Kokawa H. Interlayer growth at interfaces of Ti/Al–1% Mn, Ti/Al–4·6%Mg and Ti/pure Al friction weld joints by post-weld heat treatment. Sci Technol Weld Join 2004;9:507–12. https://doi.org/10.1179/136217104225021797.
[149] Meisnar M, Baker S, Bennett JM, Bernad A, Mostafa A, Resch S, Fernandes N, Norman A. Microstructural characterisation of rotary friction welded AA6082 and Ti-6Al-4V dissimilar joints. Mater Des 2017;132:188–97. https://doi.org/10.1016/j.matdes.2017.07.004.
[150] Gupta SP. Intermetallic compounds in diffusion couples of Ti with an Al–Si eutectic alloy. Mater Char 2002;49:321–30. https://doi.org/10.1016/S1044-5803(02)00342-X.
[151] Ma Z, Zhao W, Yan J, Li D. Interfacial reaction of intermetallic compounds of ultrasonic-assisted brazed joints between dissimilar alloys of Ti6Al4V and Al4Cu1Mg. Ultrason Sonochem 2011;18:1062–7. https://doi.org/10.1016/j.ultsonch.2011.03.025.
[152] Korolev MP, Kuz'min EV, Lysak VI, Kuz'min SV, Kharlamov VO. Structure and properties of titanium/aluminum–magnesium alloy explosive welds. Russ Metall 2024;2024:1084–90. https://doi.org/10.1134/S0036029524702057.
[153] Kar A, Kailas SV, Suwas S. Effect of zinc interlayer in microstructure evolution and mechanical properties in dissimilar friction stir welding of aluminum to titanium. J Mater Eng Perform 2018;27:6016–26. https://doi.org/10.1007/s11665-018-3697-8.
[154] Kar A, Suwas S, Kailas SV. Microstructural modification and high-temperature grain stability of aluminum in an aluminum-titanium friction stir weld with zinc interlayer. J Occup Med 2019;71:444–51. https://doi.org/10.1007/s11837-018-3152-1.
[155] Ugurlu M, Cakan A. Dissimilar friction stir butt welding of AA7075-T6 Al and Ti6Al4V Ti plates: mechanical and metallurgical analysis. Int J Adv Manuf Technol 2023;128:3491–506. https://doi.org/10.1007/s00170-023-12114-5.
[156] Amirov AI, Sidorov EA, Chumaevskii AV, Kolubaev EA, Beloborodov VA, Semenchuk NV. Impact of tool rotation speed on boundary structure and properties of AA7075 aluminum alloy and Grade 5 titanium alloy joints during friction stir welding. Russ Phys J 2024;67:2257–64. https://doi.org/10.1007/s11182-025-03372-9.
[157] Xia Z, Wang H, Shi C, Sun Z, Wang Q, Luo X. Analysis and characterization of three charge thicknesses in TA1/Al1060/Al7075 explosive welding composite process. Crystals 2023;13:1079. https://doi.org/10.3390/cryst13071079.
[158] Karpets M, Milman Y, Barabash O, Korzhova N, Senkov O, Miracle D, Legkaya T, Voskoboynik I. The influence of Zr alloying on the structure and properties of Al 3 Ti. Intermetallics 2003;11:241–9. https://doi.org/10.1016/S0966-9795(02)00234-0.
[159] Lv S, Cui Q, Huang Y, Jing X. Influence of Zr addition on TIG welding–brazing of Ti–6Al–4V toAl5A06. Mater Sci Eng, A 2013;568:150–4. https://doi.org/10.1016/j.msea.2013.01.047.

Felix Grassel is a PhD candidate at Leuphana University Lüneburg since 2021, investigating friction fsir welding of aluminium and titanium alloys. He studied mechanical engineering at the Technical University Ilmenau. After obtaining his master's degrees, he was working on Friction Stir Welding of various alloys for aeronautical and railway applications within the Solid State Materials Processing department at Helmholtz-Zentrum Hereon. His research interest includes welding and joining of similar and dissimilar materials.

Lasse Malaske is a PhD candidate at Leuphana University Lüneburg since 2022, working on refill friction stir spot welding of aluminum and titanium. Currently he is employed at Helmholtz-Zentrum Hereon within the Institute of Material and Process Design. Prior to the PhD candidate position, Lasse Malaske did his Bachelor of Engineering and Master of Engineering at Hochschule Wismar, starting in 2016. His research interest includes predominantly welding and joining of similar and dissimilar materials.

Marius Hoffmann obtained his PhD from Leuphana University Lüneburg in 2025 in the area of solid-state additive manufacturing. He graduated in 2020 from Technical University of Darmstadt, where he obtained his bachelor's and master's degrees. Afterwards he joined the Solid State Materials Processing department at Helmholtz-Zentrum Hereon. His research interests include in particular friction surfacing of similar and dissimilar material combinations.

Benjamin Klusemann is Professor of Materials Mechanics at the Leuphana University Lüneburg since 2015. Additionally, he is head of the department "Solid State Materials Processing" at the Helmholtz-Zentrum Hereon within the Institute of Material and Process Design. After his diploma in Mechanical Engineering and the Dr.-Ing. in Mechanics at the TU Dortmund in 2010, he moved for two years to RWTH Aachen before he joined TU Hamburg. With a Feodor Lynen Research Fellowship of the Humboldt foundation, he spent 9 months at the California Institute of Technology, USA in 2013. His research interests include various topics in the field of solid-state materials processing, micromechanics and multi-scale modelling, crystal plasticity, technological process simulations and experimental-modelling correlations.